

Towards a complete study of central exclusive production of K^+K^- pairs in proton-proton collisions within the tensor Pomeron approach

Piotr Lebiedowicz,^{1,*} Otto Nachtmann,^{2,†} and Antoni Szczurek^{1,‡}

¹*Institute of Nuclear Physics Polish Academy of Sciences,
Radzikowskiego 152, PL-31-342 Kraków, Poland*

²*Institut für Theoretische Physik, Universität Heidelberg,
Philosophenweg 16, D-69120 Heidelberg, Germany*



(Received 26 April 2018; published 2 July 2018)

We present a study of the central exclusive production of the K^+K^- pairs in proton-proton collisions at high energies. We consider diffractive mechanisms including the K^+K^- continuum, the dominant scalar $f_0(980)$, $f_0(1500)$, $f_0(1710)$ and tensor $f_2(1270)$, $f_2'(1525)$ resonances decaying into the K^+K^- pairs. We include also photoproduction mechanisms for the nonresonant (Drell-Söding) and the $\phi(1020)$ resonance contributions. The theoretical results are calculated within the tensor-Pomeron approach including both Pomeron and Reggeon exchanges. Predictions for planned or current experiments at RHIC and LHC are presented. We discuss the influence of the experimental cuts on the integrated cross section and on various differential distributions for outgoing particles. The distributions in two-kaon invariant mass, in a special “glueball filter variable,” as well as examples of angular distributions in the K^+K^- rest frame are presented. We compare the $\phi(1020)$ and continuum photoproduction contributions to the $f_0(980)$ and continuum diffractive contributions and discuss whether the $\phi(1020)$ resonance could be extracted experimentally. For the determination of some model parameters we also include a discussion of K -nucleon scattering, in particular total cross sections, and of $\phi(1020)$ photoproduction.

DOI: [10.1103/PhysRevD.98.014001](https://doi.org/10.1103/PhysRevD.98.014001)

I. INTRODUCTION

Diffractive exclusive production of light mesons mediated by double Pomeron exchange is expected to be an ideal process for the investigation of gluonic bound states (glueballs) due to the gluonic nature of the pomeron. Such processes were studied extensively at CERN starting from the Intersecting Storage Rings (ISR) experiments [1–6], later at the Super Proton Synchrotron (SPS) in fixed-target experiments by the WA76 and WA102 collaborations [7–14], and more recently by the COMPASS collaboration [15,16]. For reviews of experimental results see for instance [17–19]. The measurement of two charged pions in $p\bar{p}$ collisions was performed by the CDF collaboration at Tevatron

[20]. Exclusive reactions are of particular interest since they can be studied in current experiments at the LHC by the ALICE, ATLAS, CMS [21], and LHCb collaborations, as well as by the STAR collaboration at RHIC [22,23]. In such experiments it is of great advantage for the theoretical analysis if the leading outgoing protons can be measured. There are several efforts to complete installation of forward proton detectors. The CMS collaboration combines efforts with the TOTEM collaboration while the ATLAS collaboration may use the ALFA sub-detectors. Also the STAR experiment at RHIC is equipped with detectors of similar type.

On the theoretical side, the main contribution to the central diffractive exclusive production at high energies can be understood as being due to the exchange of two pomerons between the external nucleons and the centrally produced hadronic system. We believe that the soft pomeron exchange can be effectively treated as an effective rank-2 symmetric-tensor exchange as introduced in [24]. In [25] it was shown that the tensor-Pomeron model is consistent with the experimental data on the helicity structure of proton-proton elastic scattering at $\sqrt{s} = 200$ GeV and small $|t|$ from the STAR experiment [26]. The paper [25] also contains some remarks on the history of the views of the Pomeron spin

*Piotr.Lebiedowicz@ifj.edu.pl

†O.Nachtmann@thphys.uni-heidelberg.de

‡Also at Faculty of Mathematics and Natural Sciences, University of Rzeszów, Pignonia 1, PL-35-310 Rzeszów, Poland; Antoni.Szczurek@ifj.edu.pl

Published by the American Physical Society under the terms of the Creative Commons Attribution 4.0 International license. Further distribution of this work must maintain attribution to the author(s) and the published article's title, journal citation, and DOI. Funded by SCOAP³.

structure. In [27] the central exclusive production of several scalar and pseudoscalar mesons in the reaction $pp \rightarrow ppM$ was studied for the relatively low WA102 energy. Then, in [28], the model was applied to the reaction $pp \rightarrow pp\pi^+\pi^-$ at high energies including the $\pi^+\pi^-$ continuum, the dominant scalar $f_0(500)$, $f_0(980)$ and tensor $f_2(1270)$ resonances decaying into the $\pi^+\pi^-$ pairs. The resonant ρ^0 and nonresonant (Drell-Söding) $\pi^+\pi^-$ photoproduction was studied in [29]. In [30], an extensive study of the reaction $\gamma p \rightarrow \pi^+\pi^-p$ was presented. The ρ^0 meson production associated with a very forward/backward πN system in the $pp \rightarrow pp\rho^0\pi^0$ and $pp \rightarrow pn\rho^0\pi^+$ processes was discussed in [31]. Also the central exclusive $\pi^+\pi^-\pi^+\pi^-$ production via the intermediate $\sigma\sigma$ and $\rho^0\rho^0$ states in pp collisions was studied in [32]. Recently, in [33], the central exclusive production of the $p\bar{p}$ in the continuum and via scalar resonances in pp collisions was studied.

Some time ago two of us considered the exclusive $pp \rightarrow ppK^+K^-$ reaction in a simple Regge-like model [34]. The Born approximation is usually not sufficient and absorption corrections have to be taken into account, see e.g. [35,36]. In [34] the production of the diffractive K^+K^- continuum and of the scalar χ_{c0} meson decaying via $\chi_{c0} \rightarrow K^+K^-$ was studied. For other related works see [37] for the $pp \rightarrow pp\pi^+\pi^-$ reaction, [38] for the exclusive $f_0(1500)$, and [39] for χ_{c0} meson production.

In [40] a model for the exclusive diffractive meson production in pp collisions was discussed based on the

convolution of the Donnachie-Landshoff parametrization of the Pomeron distribution in the proton with the Pomeron-Pomeron-meson total cross section. In this approach the cross section is calculated by summing over the direct-channel contributions from the pomeron and two different f_1 and f_2 trajectories associated to the glueball candidate $f_0(980)$ and the $f_2(1270)$ resonances, respectively. Also the $f_0(500)$ resonance contribution dominating the small mass region and a slowly increasing background were taken into account. The absolute contribution of resonances, e.g. of the $f_0(980)$ and the $f_2(1270)$, to the total cross section cannot be derived within this approach, and must hence be deduced from experimental data. But the relative weights of the various resonances on one trajectory are correlated by the duality argument made in [40].

The aim of the study presented here is the application of the tensor-Pomeron model to central exclusive production of K^+K^- pairs in pp collisions. We wish to show first predictions in the tensor-Pomeron approach for the production of the diffractive K^+K^- continuum, of the scalar $f_0(980)$, $f_0(1500)$, $f_0(1710)$, and the tensor $f_2(1270)$, $f_2'(1525)$ resonances decaying into K^+K^- pairs. This model, being formulated at the amplitude level, allows us also to calculate interference effects of the various contributions. In the following we wish to show differential distributions which can be helpful in the investigation of scalar and tensor resonance parameters. Therefore, we shall treat each resonance in its own right and shall not *a priori* suppose any correlations of the coupling parameters of different resonances. In addition the resonant $\phi(1020)$ and nonresonant (Drell-Söding) K^+K^- photoproduction mechanisms will be discussed. So far the cross sections for the exclusive $pp \rightarrow pp\phi(1020)$ reaction were calculated within a pQCD k_t -factorization approach [41], and in a color dipole approach [42,43].

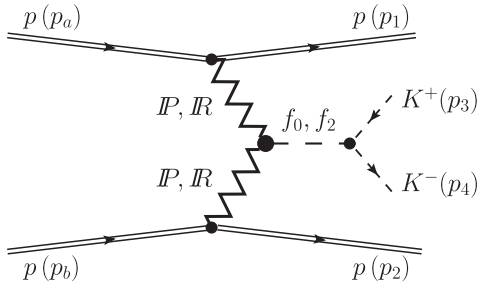


FIG. 1. The Born diagram for double-Pomeron/Reggeon central exclusive scalar and tensor resonances production and their subsequent decays into K^+K^- in proton-proton collisions.

II. EXCLUSIVE K^+K^- PRODUCTION

We study central exclusive production of K^+K^- in proton-proton collisions at high energies

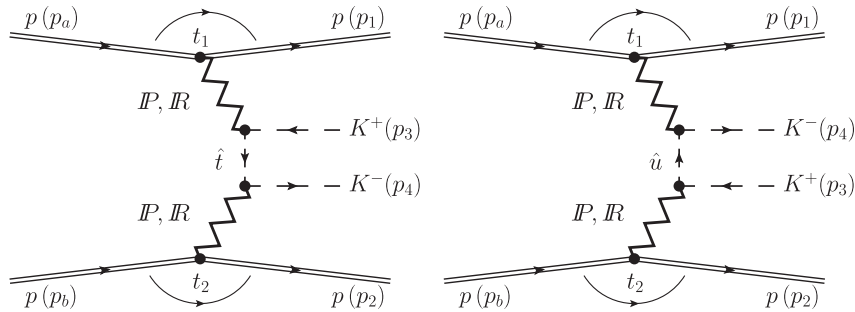


FIG. 2. The Born diagrams for double-Pomeron/Reggeon central exclusive K^+K^- continuum production in proton-proton collisions.

TABLE I. A list of resonances, up to a mass of 1800 MeV, that decay into K^+K^- and/or $\pi^+\pi^-$. The meson masses, their total widths Γ and branching fractions are taken from PDG [44].

Meson	$I^G J^{PC}$	m (MeV)	Γ (MeV)	$\Gamma_{K\bar{K}}/\Gamma$	$\Gamma_{\pi\pi}/\Gamma$	Other decay modes
$f_0(500)$	0^+0^{++}	400–550	400–700	-	Dominant	$\gamma\gamma$
$\rho(770)$	1^+1^{--}	769.0 ± 1.0	151.7 ± 2.6	-	$\frac{\Gamma_{\pi^+\pi^-}}{\Gamma} = 1$	
$f_0(980)$	0^+0^{++}	990 ± 20	10–100	Seen	Dominant	$\gamma\gamma$
$a_0(980)$	1^-0^{++}	980 ± 20	50–100	Seen	-	$\eta\pi, \gamma\gamma$
$\phi(1020)$	0^-1^{--}	1019.460 ± 0.016	4.247 ± 0.016	$\frac{\Gamma_{K^+K^-}}{\Gamma} = 0.489 \pm 0.005$	-	$K_L^0 K_S^0, 3\pi, \eta\gamma$
$f_2(1270)$	0^+2^{++}	1275.5 ± 0.8	$186.7^{+2.2}_{-2.5}$	$0.046^{+0.005}_{-0.004}$	$0.842^{+0.029}_{-0.009}$	$4\pi, \gamma\gamma$
$a_2(1320)$	1^-2^{++}	1318.1 ± 0.7	109.8 ± 2.4	0.049 ± 0.008	-	$3\pi, \eta\pi, \omega\pi\pi, \gamma\gamma$
$f_0(1370)$	0^+0^{++}	1200–1500	200–500	Seen	Seen	4π ($\rho\rho$), $\eta\eta, \gamma\gamma$
$a_0(1450)$	1^-0^{++}	1474 ± 19	265 ± 13	0.082 ± 0.028	-	$\pi\eta, \pi\eta'(958), \gamma\gamma$
$f_0(1500)$	0^+0^{++}	1504 ± 6	109 ± 7	0.086 ± 0.010	0.349 ± 0.023	$4\pi, \eta\eta, \eta\eta'(958)$
$f_2'(1525)$	0^+2^{++}	1525 ± 5	73^{+6}_{-5}	0.887 ± 0.022	$(8.2 \pm 1.5) \times 10^{-3}$	$\eta\eta, \gamma\gamma$
$f_2(1640)$	0^+2^{++}	1639 ± 6	99^{+60}_{-40}	Seen	-	$4\pi, \omega\omega$
$\phi(1680)$	0^-1^{--}	1680 ± 20	150 ± 50	Seen	-	$K\bar{K}^*$ (892)
$\rho_3(1690)$	1^+3^{--}	1696 ± 4	204 ± 18	0.0158 ± 0.0026	0.236 ± 0.013	$4\pi, K\bar{K}\pi$
$\rho(1700)$	1^+1^{--}	1740.8 ± 22.2	187.2 ± 26.7	Seen	Seen	4π ($\rho\pi\pi$)
$a_2(1700)$	1^-2^{++}	1732 ± 16	194 ± 40	Seen	-	$\eta\pi$
$f_0(1710)$	0^+0^{++}	1723^{+6}_{-5}	139 ± 8	Seen	Seen	$\eta\eta, \omega\omega$

$$p(p_a, \lambda_a) + p(p_b, \lambda_b) \rightarrow p(p_1, \lambda_1) + K^+(p_3) + K^-(p_4) + p(p_2, \lambda_2), \quad (2.1)$$

where $p_{a,b}, p_{1,2}$ and $\lambda_{a,b}, \lambda_{1,2} \in \{+1/2, -1/2\}$, indicated in brackets, denote the four-momenta and helicities of the protons, and $p_{3,4}$ denote the four-momenta of the charged kaons, respectively.

The full amplitude of K^+K^- production is a sum of the continuum amplitude and the amplitudes with the s -channel resonances:

$$\mathcal{M}_{pp \rightarrow ppK^+K^-} = \mathcal{M}_{pp \rightarrow ppK^+K^-}^{KK\text{-continuum}} + \mathcal{M}_{pp \rightarrow ppK^+K^-}^{KK\text{-resonances}}. \quad (2.2)$$

The amplitude for exclusive resonant K^+K^- production via the Pomeron-Pomeron fusion, shown by the diagram of Fig. 1, can be written as

$$\mathcal{M}_{pp \rightarrow ppK^+K^-}^{KK\text{-resonances}} = \mathcal{M}_{pp \rightarrow ppK^+K^-}^{(\mathbb{P}\mathbb{P} \rightarrow f_0 \rightarrow K^+K^-)} + \mathcal{M}_{pp \rightarrow ppK^+K^-}^{(\mathbb{P}\mathbb{P} \rightarrow f_2 \rightarrow K^+K^-)}. \quad (2.3)$$

As indicated in Fig. 1 also contributions involving non-leading Reggeons \mathbb{R} : $\rho_{\mathbb{R}}$ (ρ Reggeon), $\omega_{\mathbb{R}}$ (ω Reggeon), $f_{2\mathbb{R}}$ (f_2 Reggeon), $a_{2\mathbb{R}}$ (a_2 Reggeon) can contribute. The relevant production modes via (C_1, C_2) fusion¹ giving resonances are listed in Table II of [28]. However, in the present paper we shall consider only resonance production

¹Here C_1 and C_2 are the charge-conjugation quantum numbers of the exchange objects and $C_1, C_2 \in \{+1, -1\}$.

by Pomeron-Pomeron fusion in order not to be swamped by too many, essentially unknown, coupling parameters.

Turning now to continuum diffractive K^+K^- production shown in Fig. 2 we have again Pomeron and Reggeon contributions. Here we will be able to extract all relevant coupling parameters from the kaon-nucleon total cross section data. Therefore, we shall include in the calculation Pomeron and Reggeon exchanges. In this way we will also get an estimate of the possible importance of the latter exchanges. In the following we treat the $C = +1$ Pomeron and the Reggeons $\mathbb{R}_+ = f_{2\mathbb{R}}, a_{2\mathbb{R}}$ as effective tensor exchanges while the $C = -1$ Reggeons $\mathbb{R}_- = \omega_{\mathbb{R}}, \rho_{\mathbb{R}}$ are treated as effective vector exchanges.

In Table I we have listed intermediate resonances that contribute to the $pp \rightarrow ppK^+K^-$ and/or $pp \rightarrow pp\pi^+\pi^-$ reactions.

III. DIFFRACTIVE CONTRIBUTIONS

A. K^+K^- continuum central production

The generic diagrams for diffractive exclusive K^+K^- continuum production are shown in Fig. 2. At high energies the exchange objects to be considered are the Pomeron \mathbb{P} and the Reggeons \mathbb{R} . The amplitude can be written as the following sum:

$$\mathcal{M}_{pp \rightarrow ppK^+K^-}^{KK\text{-continuum}} = \mathcal{M}^{(\mathbb{P}\mathbb{P} \rightarrow K^+K^-)} + \mathcal{M}^{(\mathbb{P}\mathbb{R} \rightarrow K^+K^-)} + \mathcal{M}^{(\mathbb{R}\mathbb{P} \rightarrow K^+K^-)} + \mathcal{M}^{(\mathbb{R}\mathbb{R} \rightarrow K^+K^-)}. \quad (3.1)$$

The $\mathbb{P}\mathbb{P}$ -exchange amplitude on the Born level can be written as the sum:

$$\mathcal{M}(\mathbb{P}\mathbb{P}\rightarrow K^+K^-) = \mathcal{M}_{\lambda_a\lambda_b\rightarrow\lambda_1\lambda_2K^+K^-}^{(\hat{i})} + \mathcal{M}_{\lambda_a\lambda_b\rightarrow\lambda_1\lambda_2K^+K^-}^{(\hat{u})}, \quad (3.2)$$

where

$$\begin{aligned} \mathcal{M}_{\lambda_a\lambda_b\rightarrow\lambda_1\lambda_2\pi^+\pi^-}^{(\hat{i})} &= (-i)\bar{u}(p_1, \lambda_1)i\Gamma_{\mu_1\nu_1}^{(\mathbb{P}pp)}(p_1, p_a)u(p_a, \lambda_a)i\Delta^{(\mathbb{P})\mu_1\nu_1, \alpha_1\beta_1}(s_{13}, t_1)i\Gamma_{\alpha_1\beta_1}^{(\mathbb{P}KK)}(p_t, -p_3)i\Delta^{(K)}(p_t) \\ &\quad \times i\Gamma_{\alpha_2\beta_2}^{(\mathbb{P}KK)}(p_4, p_t)i\Delta^{(\mathbb{P})\alpha_2\beta_2, \mu_2\nu_2}(s_{24}, t_2)\bar{u}(p_2, \lambda_2)i\Gamma_{\mu_2\nu_2}^{(\mathbb{P}pp)}(p_2, p_b)u(p_b, \lambda_b), \end{aligned} \quad (3.3)$$

$$\begin{aligned} \mathcal{M}_{\lambda_a\lambda_b\rightarrow\lambda_1\lambda_2\pi^+\pi^-}^{(\hat{u})} &= (-i)\bar{u}(p_1, \lambda_1)i\Gamma_{\mu_1\nu_1}^{(\mathbb{P}pp)}(p_1, p_a)u(p_a, \lambda_a)i\Delta^{(\mathbb{P})\mu_1\nu_1, \alpha_1\beta_1}(s_{14}, t_1)i\Gamma_{\alpha_1\beta_1}^{(\mathbb{P}KK)}(p_4, p_u)i\Delta^{(K)}(p_u) \\ &\quad \times i\Gamma_{\alpha_2\beta_2}^{(\mathbb{P}KK)}(p_u, -p_3)i\Delta^{(\mathbb{P})\alpha_2\beta_2, \mu_2\nu_2}(s_{23}, t_2)\bar{u}(p_2, \lambda_2)i\Gamma_{\mu_2\nu_2}^{(\mathbb{P}pp)}(p_2, p_b)u(p_b, \lambda_b). \end{aligned} \quad (3.4)$$

Here $p_t = p_a - p_1 - p_3$ and $p_u = p_4 - p_a + p_1$, $s_{ij} = (p_i + p_j)^2$. The normal kaon propagator is $i\Delta^{(K)}(k) = i/(k^2 - m_K^2)$. Furthermore $\Delta^{(\mathbb{P})}$ and $\Gamma^{(\mathbb{P}pp)}$ denote the effective propagator and proton vertex function, respectively, for the tensorial Pomeron. The propagator of the tensor-Pomeron exchange is written as (see Eq. (3.10) of [24]):

$$i\Delta_{\mu\nu, \kappa\lambda}^{(\mathbb{P})}(s, t) = \frac{1}{4s} \left(g_{\mu\kappa}g_{\nu\lambda} + g_{\mu\lambda}g_{\nu\kappa} - \frac{1}{2}g_{\mu\nu}g_{\kappa\lambda} \right) (-is\alpha'_{\mathbb{P}})^{\alpha_{\mathbb{P}}(t)-1} \quad (3.5)$$

and fulfills the following relations

$$\Delta_{\mu\nu, \kappa\lambda}^{(\mathbb{P})}(s, t) = \Delta_{\nu\mu, \kappa\lambda}^{(\mathbb{P})}(s, t) = \Delta_{\mu\nu, \lambda\kappa}^{(\mathbb{P})}(s, t) = \Delta_{\kappa\lambda, \mu\nu}^{(\mathbb{P})}(s, t), \quad g^{\mu\nu}\Delta_{\mu\nu, \kappa\lambda}^{(\mathbb{P})}(s, t) = 0, \quad g^{\kappa\lambda}\Delta_{\mu\nu, \kappa\lambda}^{(\mathbb{P})}(s, t) = 0. \quad (3.6)$$

Here the Pomeron trajectory $\alpha_{\mathbb{P}}(t)$ is assumed to be of standard linear form, see e.g. [45,46],

$$\alpha_{\mathbb{P}}(t) = \alpha_{\mathbb{P}}(0) + \alpha'_{\mathbb{P}}t, \quad \alpha_{\mathbb{P}}(0) = 1.0808, \quad \alpha'_{\mathbb{P}} = 0.25 \text{ GeV}^{-2}. \quad (3.7)$$

The Pomeron-proton vertex function is written as (see Eq. (3.43) of [24])

$$i\Gamma_{\mu\nu}^{(\mathbb{P}pp)}(p', p) = i\Gamma_{\mu\nu}^{(\mathbb{P}\bar{p}\bar{p})}(p', p) = -i3\beta_{\mathbb{P}NN}F_1((p' - p)^2) \left\{ \frac{1}{2}[\gamma_{\mu}(p' + p)_{\nu} + \gamma_{\nu}(p' + p)_{\mu}] - \frac{1}{4}g_{\mu\nu}(\not{p}' + \not{p}) \right\}, \quad (3.8)$$

where $\beta_{\mathbb{P}NN} = 1.87 \text{ GeV}^{-1}$. The $\mathbb{P}KK$ vertices in the amplitudes (3.3) and (3.4) can be written in analogy to the $\mathbb{P}\pi\pi$ vertices (see (3.45) of [24]) but with the replacement $\beta_{\mathbb{P}\pi\pi} \rightarrow \beta_{\mathbb{P}KK}$,

$$i\Gamma_{\mu\nu}^{(\mathbb{P}KK)}(k', k) = -i2\beta_{\mathbb{P}KK} \left[(k' + k)_{\mu}(k' + k)_{\nu} - \frac{1}{4}g_{\mu\nu}(k' + k)^2 \right] F_M((k' - k)^2). \quad (3.9)$$

The form factors, taking into account that the hadrons are extended objects, are chosen as

$$F_1(t) = \frac{4m_p^2 - 2.79t}{(4m_p^2 - t)(1 - t/m_D^2)^2}, \quad F_M(t) = \frac{1}{1 - t/\Lambda_0^2}, \quad \hat{F}_K(k^2) = \frac{\Lambda_{\text{off},M}^2 - m_K^2}{\Lambda_{\text{off},M}^2 - k^2}, \quad (3.10)$$

where m_p is the proton mass and $m_D^2 = 0.71 \text{ GeV}^2$ is the dipole mass squared and $\Lambda_0^2 = 0.5 \text{ GeV}^2$; see Eqs. (3.29) and (3.34) of [24], respectively.

The off-shellness of the intermediate kaons is taken into account by the inclusion of form factors. The form factors are normalized to unity at the on-shell point $\hat{F}_K(m_K^2) = 1$ and parametrized here in the monopole form

where $\Lambda_{\text{off},M}$ could be adjusted to experimental data. We take $\Lambda_{\text{off},M} = 0.7 \text{ GeV}$, that is, the same value as for the pion off-shell form factor in the reaction $pp \rightarrow pp\pi^+\pi^-$ discussed in [28]. In [28] we fixed a parameter of the form factor for off-shell pion and a few parameters of the Pomeron-Pomeron-meson coupling constants to describe the CDF data [20]; see Fig. 9 of [28].

In our calculations we include both the tensor-Pomeron and the Reggeon \mathbb{R}_+ and \mathbb{R}_- exchanges. In the following we collect the expressions for Reggeon effective propagators and vertex functions in order to make our present paper self contained. For extensive discussions motivating the following expressions we refer to Sec. III of [24].

The ansatz for the $C = +1$ Reggeons $\mathbb{R}_+ = f_{2\mathbb{R}}, a_{2\mathbb{R}}$ is similar to (3.5)–(3.8). The \mathbb{R}_+ propagator is obtained from (3.5) with the replacements

$$\begin{aligned}\alpha_{\mathbb{P}}(t) &\rightarrow \alpha_{\mathbb{R}_+}(t) = \alpha_{\mathbb{R}_+}(0) + \alpha'_{\mathbb{R}_+} t, \\ \alpha_{\mathbb{R}_+}(0) &= 0.5475, \\ \alpha'_{\mathbb{R}_+} &= 0.9 \text{ GeV}^{-2}.\end{aligned}\quad (3.12)$$

In (3.12) and in the following the parameters of the Reggeon trajectories are taken from [46]. The $f_{2\mathbb{R}}$ - and $a_{2\mathbb{R}}$ -proton vertex functions are obtained from (3.8) with the replacements

$$\begin{aligned}3\beta_{\mathbb{P}NN} &\rightarrow \frac{g_{f_{2\mathbb{R}}PP}}{M_0}, \\ g_{f_{2\mathbb{R}}PP} &= 11.04,\end{aligned}\quad (3.13)$$

and

$$\begin{aligned}3\beta_{\mathbb{P}NN} &\rightarrow \frac{g_{a_{2\mathbb{R}}PP}}{M_0}, \\ g_{a_{2\mathbb{R}}PP} &= 1.68,\end{aligned}\quad (3.14)$$

respectively. In (3.13), (3.14) and in the following $M_0 = 1 \text{ GeV}$ is used in various places for dimensional reasons. The $f_{2\mathbb{R}}$ - and $a_{2\mathbb{R}}$ -kaon vertex functions are obtained from (3.9) with the replacements

$$2\beta_{\mathbb{P}KK} \rightarrow \frac{g_{f_{2\mathbb{R}}KK}}{2M_0}, \quad (3.15)$$

$$2\beta_{\mathbb{P}KK} \rightarrow \frac{g_{a_{2\mathbb{R}}KK}}{2M_0}, \quad (3.16)$$

respectively. For the $C = -1$ Reggeons $\mathbb{R}_- = \omega_{\mathbb{R}}, \rho_{\mathbb{R}}$ we assume an effective vector propagator (see Eqs. (3.14)–(3.15) of [24])

$$i\Delta_{\mu\nu}^{(\mathbb{R}_-)}(s, t) = ig_{\mu\nu} \frac{1}{M_-^2} (-is\alpha'_{\mathbb{R}_-})^{\alpha_{\mathbb{R}_-}(t)-1}, \quad (3.17)$$

with

$$\begin{aligned}\alpha_{\mathbb{R}_-}(t) &= \alpha_{\mathbb{R}_-}(0) + \alpha'_{\mathbb{R}_-} t, \\ \alpha_{\mathbb{R}_-}(0) &= 0.5475, \\ \alpha'_{\mathbb{R}_-} &= 0.9 \text{ GeV}^{-2},\end{aligned}\quad (3.18)$$

$$M_- = 1.41 \text{ GeV}. \quad (3.19)$$

The value of (3.19) is taken from [24] as default value for the parameter of the propagators for $\omega_{\mathbb{R}}$ and $\rho_{\mathbb{R}}$ exchanges.

For the \mathbb{R}_- -proton vertices we have (see Eqs. (3.59)–(3.62) of [24])

$$\begin{aligned}i\Gamma_{\mu}^{(\omega_{\mathbb{R}}PP)}(p', p) &= i\Gamma_{\mu}^{(\omega_{\mathbb{R}}nn)}(p', p) = -i\Gamma_{\mu}^{(\omega_{\mathbb{R}}\bar{p}\bar{p})}(p', p) \\ &= -ig_{\omega_{\mathbb{R}}PP} F_1((p' - p)^2) \gamma_{\mu},\end{aligned}\quad (3.20)$$

$$\begin{aligned}i\Gamma_{\mu}^{(\rho_{\mathbb{R}}PP)}(p', p) &= -i\Gamma_{\mu}^{(\rho_{\mathbb{R}}nn)}(p', p) = -i\Gamma_{\mu}^{(\rho_{\mathbb{R}}\bar{p}\bar{p})}(p', p) \\ &= -ig_{\rho_{\mathbb{R}}PP} F_1((p' - p)^2) \gamma_{\mu},\end{aligned}\quad (3.21)$$

with

$$\begin{aligned}g_{\omega_{\mathbb{R}}PP} &= 8.65, \\ g_{\rho_{\mathbb{R}}PP} &= 2.02,\end{aligned}\quad (3.22)$$

respectively. Note that in (3.21) the vertex function for the isospin 1 $\rho_{\mathbb{R}}$ Reggeon changes sign when we replace protons by neutrons. This is also the case for the isospin 1 $a_{2\mathbb{R}}$ Reggeon exchange; see (3.51) of [24]. The \mathbb{R}_- -kaon vertex ($\mathbb{R}_- = \omega_{\mathbb{R}}, \rho_{\mathbb{R}}$) can be written in analogy to the $\rho_{\mathbb{R}}$ -pion vertex (see (3.63) of [24])

$$\begin{aligned}i\Gamma_{\mu}^{(\mathbb{R}_-K^+K^+)}(k', k) &= -i\Gamma_{\mu}^{(\mathbb{R}_-K^-K^-)}(k', k) \\ &= -\frac{i}{2} g_{\mathbb{R}_-KK} F_M((k' - k)^2) (k' + k)_{\mu}.\end{aligned}\quad (3.23)$$

To obtain the Pomeron/Reggeon-kaon coupling constants we consider the following elastic scattering processes at high energies

$$K^{\pm}(p_1) + p(p_2, \lambda_2) \rightarrow K^{\pm}(p_3) + p(p_4, \lambda_4), \quad (3.24)$$

$$K^{\pm}(p_1) + n(p_2, \lambda_2) \rightarrow K^{\pm}(p_3) + n(p_4, \lambda_4). \quad (3.25)$$

We treat (3.24) and (3.25) in analogy to the elastic $\pi^{\pm}p$ scattering; see section VII of [24]. For the case of the elastic kaon-nucleon scattering amplitudes we set for p and n also $N(I_3)$ with $I_3 = +1/2$ and $I_3 = -1/2$, respectively. We obtain

$$\begin{aligned}
\langle K^\pm(p_3), N(I_3, p_4, \lambda_4) | T | K^\pm(p_1), N(I_3, p_2, \lambda_2) \rangle &= i2s\delta_{\lambda_4\lambda_2} F_1(t) F_M(t) \left\{ 6\beta_{\mathbb{P}KK}\beta_{\mathbb{P}NN}(-is\alpha_{\mathbb{P}}')^{\alpha_{\mathbb{P}}(t)-1} \right. \\
&+ \frac{1}{2} [g_{f_{2\mathbb{R}}KK}g_{f_{2\mathbb{R}}PP} + (-1)^{I_3-\frac{1}{2}}g_{a_{2\mathbb{R}}KK}g_{a_{2\mathbb{R}}PP}] M_0^{-2} (-is\alpha'_{\mathbb{R}+})^{\alpha_{\mathbb{R}+}(t)-1} \\
&\left. \pm \frac{i}{2} [g_{\omega_{\mathbb{R}}KK}g_{\omega_{\mathbb{R}}PP} + (-1)^{I_3-\frac{1}{2}}g_{\rho_{\mathbb{R}}KK}g_{\rho_{\mathbb{R}}PP}] M_0^{-2} (-is\alpha'_{\mathbb{R}-})^{\alpha_{\mathbb{R}-}(t)-1} \right\}. \tag{3.26}
\end{aligned}$$

Here we have $s = (p_1 + p_2)^2$ and $t = (p_1 - p_3)^2$ and we work in the approximation $s \gg |t|, m_p^2$.

For the total cross sections we obtain from the optical theorem for large s

$$\begin{aligned}
\sigma_{\text{tot}}(K^\pm, N(I_3)) &= \frac{1}{2s} \sum_{\lambda_2} \text{Im} \langle K^\pm(p_1), N(I_3, p_2, \lambda_2) | T | K^\pm(p_1), N(I_3, p_2, \lambda_2) \rangle \\
&= 2 \left\{ 6\beta_{\mathbb{P}KK}\beta_{\mathbb{P}NN} \cos \left[\frac{\pi}{2} (\alpha_{\mathbb{P}}(0) - 1) \right] (s\alpha'_{\mathbb{P}})^{\alpha_{\mathbb{P}}(0)-1} \right. \\
&+ \frac{1}{2} [g_{f_{2\mathbb{R}}KK}g_{f_{2\mathbb{R}}PP} + (-1)^{I_3-\frac{1}{2}}g_{a_{2\mathbb{R}}KK}g_{a_{2\mathbb{R}}PP}] M_0^{-2} \cos \left[\frac{\pi}{2} (\alpha_{\mathbb{R}+}(0) - 1) \right] (s\alpha'_{\mathbb{R}+})^{\alpha_{\mathbb{R}+}(0)-1} \\
&\left. \mp \frac{1}{2} [g_{\omega_{\mathbb{R}}KK}g_{\omega_{\mathbb{R}}PP} + (-1)^{I_3-\frac{1}{2}}g_{\rho_{\mathbb{R}}KK}g_{\rho_{\mathbb{R}}PP}] M_0^{-2} \cos \left[\frac{\pi}{2} \alpha_{\mathbb{R}-}(0) \right] (s\alpha'_{\mathbb{R}-})^{\alpha_{\mathbb{R}-}(0)-1} \right\}. \tag{3.27}
\end{aligned}$$

Following Donnachie and Landshoff [45] we use a two component parametrization for the total cross sections of kaon-nucleon scattering

$$\sigma_{\text{tot}}(a, b) = X_{ab}(sM_0^{-2})^{0.0808} + Y_{ab}(sM_0^{-2})^{-0.4525}. \tag{3.28}$$

Here $(a, b) = (K^+, p), (K^-, p), (K^+, n), (K^-, n)$, and $M_0 = 1 \text{ GeV}$. The numbers $X_{ab} \equiv X$ and Y_{ab} are

$$\begin{aligned}
X &= 11.93 \text{ mb} \hat{=} 30.64 \text{ GeV}^{-2}, \\
Y_{K^+p} &= 7.58 \text{ mb} \hat{=} 19.47 \text{ GeV}^{-2}, \\
Y_{K^-p} &= 25.33 \text{ mb} \hat{=} 65.05 \text{ GeV}^{-2}, \\
Y_{K^+n} &= 9.08 \text{ mb} \hat{=} 23.32 \text{ GeV}^{-2}, \\
Y_{K^-n} &= 19.09 \text{ mb} \hat{=} 49.03 \text{ GeV}^{-2}, \tag{3.29}
\end{aligned}$$

where the values for the X, Y_{K^+p} and Y_{K^-p} are taken from Fig. 3.2 of [46] and the values for the Y_{K^+n} and Y_{K^-n} are from our fit to the world data from [44].

We compare now (3.27) with (3.28) taking into account the parameters of the Pomeron and Reggeon trajectories and of their vertices from [24] quoted above in Eqs. (3.5) to (3.22). We get then the following results for the couplings

$$\beta_{\mathbb{P}KK} = 1.54 \text{ GeV}^{-1}, \tag{3.30}$$

$$\begin{aligned}
g_{f_{2\mathbb{R}}KK} &= 4.47, & g_{a_{2\mathbb{R}}KK} &= 2.28, \\
g_{\omega_{\mathbb{R}}KK} &= 5.99, & g_{\rho_{\mathbb{R}}KK} &= 7.15. \tag{3.31}
\end{aligned}$$

B. Scalar mesons central production

The K^+K^- production amplitude through the s -channel exchange of scalar mesons, such as $f_0(980), f_0(1370), f_0(1500)$, and $f_0(1710)$, via the $\mathbb{P}\mathbb{P}$ fusion can be written as

$$\begin{aligned}
\mathcal{M}_{\lambda_a\lambda_b \rightarrow \lambda_1\lambda_2 K^+K^-}^{(\mathbb{P}\mathbb{P} \rightarrow f_0 \rightarrow K^+K^-)} &= (-i)\bar{u}(p_1, \lambda_1) i\Gamma_{\mu_1\nu_1}^{(\mathbb{P}\mathbb{P})}(p_1, p_a) u(p_a, \lambda_a) \\
&\times i\Delta^{(\mathbb{P})\mu_1\nu_1, \alpha_1\beta_1}(s_1, t_1) \\
&\times i\Gamma_{\alpha_1\beta_1, \alpha_2\beta_2}^{(\mathbb{P}\mathbb{P}f_0)}(q_1, q_2) i\Delta^{(f_0)}(p_{34}) \\
&\times i\Gamma^{(f_0KK)}(p_3, p_4) i\Delta^{(\mathbb{P})\alpha_2\beta_2, \mu_2\nu_2}(s_2, t_2) \\
&\times \bar{u}(p_2, \lambda_2) i\Gamma_{\mu_2\nu_2}^{(\mathbb{P}\mathbb{P})}(p_2, p_b) u(p_b, \lambda_b), \tag{3.32}
\end{aligned}$$

where $s_1 = (p_a + q_2)^2 = (p_1 + p_{34})^2, s_2 = (p_b + q_1)^2 = (p_2 + p_{34})^2$, and $p_{34} = p_3 + p_4$. The effective Lagrangians and the vertices for the fusion of two tensor Pomerons into the f_0 meson were discussed in Appendix A of [27]. The $\mathbb{P}\mathbb{P}f_0$ vertex, including a form factor, reads as follows ($p_{34} = q_1 + q_2$)

$$\begin{aligned}
i\Gamma_{\mu\nu, \kappa\lambda}^{(\mathbb{P}\mathbb{P}f_0)}(q_1, q_2) &= (i\Gamma_{\mu\nu, \kappa\lambda}^{(\mathbb{P}\mathbb{P}f_0)})|_{\text{bare}} + i\Gamma_{\mu\nu, \kappa\lambda}^{\prime\prime(\mathbb{P}\mathbb{P}f_0)}(q_1, q_2)|_{\text{bare}} \\
&\times \tilde{F}^{(\mathbb{P}\mathbb{P}f_0)}(q_1^2, q_2^2, p_{34}^2); \tag{3.33}
\end{aligned}$$

see (A.21) of [27]. The vertex (3.33) contains two independent $\mathbb{P}\mathbb{P}f_0$ couplings corresponding to the lowest allowed values of (l, S) , that is $(l, S) = (0, 0)$ and $(2, 2)$.

We take the factorized form for the $\mathbb{P}\mathbb{P}f_0$ form factor

$$\tilde{F}^{(\mathbb{P}\mathbb{P}f_0)}(q_1^2, q_2^2, p_{34}^2) = F_M(q_1^2)F_M(q_2^2)F^{(\mathbb{P}\mathbb{P}f_0)}(p_{34}^2) \quad (3.34)$$

normalised to $\tilde{F}^{(\mathbb{P}\mathbb{P}f_0)}(0, 0, m_{f_0}^2) = 1$. In practical calculations we take

$$F^{(\mathbb{P}\mathbb{P}f_0)}(p_{34}^2) = \exp\left(\frac{-(p_{34}^2 - m_{f_0}^2)^2}{\Lambda_{f_0}^4}\right),$$

$$\Lambda_{f_0} = 1 \text{ GeV}. \quad (3.35)$$

There has been a long history of uncertainty about the properties of the $f_0(1710)$ meson, one of the earliest glueball candidates. This state was observed in the WA76 experiment at $\sqrt{s} = 23.8$ GeV [7] in both the K^+K^- and $K_S^0K_S^0$ channels in the dikaon invariant mass region around 1.7 GeV. By studying the K^+K^- angular distributions the authors of [7] found that the so called $\theta/f_J(1720)$ state has $J^{PC} = 2^{++}$. In [11] a reanalysis of the K^+K^- channel from the WA76 experiment was performed. A partial wave analysis of the centrally produced K^+K^- system, as performed in [11] (see Fig. 4 there), shows in the S -wave a threshold enhancement and a structure in the 1.5–1.7 GeV mass interval which has been interpreted as being due to the $f_0(1500)$ and $f_J(1710)$ with $J = 0$. The D -wave shows peaks in the 1.3 GeV and 1.5 GeV mass regions, presumably due to the $f_2(1270)/a_2(1320)$ and $f_2'(1525)$ resonances. In the D -wave at higher masses there is no evidence for any significant structure in the 1.7 GeV mass region and only a wide structure around 2.2 GeV is seen that may be due to the $f_2(2150)$ meson. In the P -wave (P_1^-) a peak corresponding to the $\phi(1020)$ is observed. These results are compatible with those coming from WA102 experiment [10] at $\sqrt{s} = 29$ GeV. The $f_J(1710)$ with $J = 2$ state has been observed also in radiative J/ψ decays [47]. However, a new analysis of $J/\psi \rightarrow \gamma K^+K^-$ and $\gamma K_S^0K_S^0$ [48] strongly demonstrates that the mass region around 1.7 GeV is predominantly 0^{++} from the $f_0(1710)$.² This conclusion is consistent with the latest central production data of WA76 and WA102 [10–12].

An important variable characterizing the production mechanisms of the various f_0 mesons is the azimuthal angle ϕ_{pp} between the outgoing protons, $p(p_1)$ and $p(p_2)$ in (2.1). As can be seen from the experimental results presented in [12,13,17] for the $f_0(980)$, $f_0(1500)$, and $f_0(1710)$ states the cross sections peak at $\phi_{pp} = 0$ in contrast to the $f_0(1370)$ meson. It was shown in [27] that the appropriate angular shapes for the central production of $f_0(980)$ and $f_0(1500)$ mesons could be obtained with the $\mathbb{P}\mathbb{P}f_0$ vertices corresponding to the sum of the two lowest values of (l, S)

²It is mentioned in [48] that the amount of the possible 2^{++} component in the 1.7 GeV mass region is of the order of a few percent.

couplings, $(l, S) = (0, 0)$ and $(2, 2)$, with appropriate coupling constants $g'_{\mathbb{P}\mathbb{P}M}$ and $g''_{\mathbb{P}\mathbb{P}M}$. For the production of $f_0(1370)$ meson the $(l, S) = (0, 0)$ coupling alone already describes the azimuthal angular correlation reasonably well. In [27] we determined the corresponding (dimensionless) $\mathbb{P}\mathbb{P}f_0$ coupling constants by approximately fitting the theoretical results to the WA102 data for the angular distributions and the total cross sections given in Table 1 of [17]. The following “preferred” values for the couplings were obtained, see Table 3 of [27], $(g'_{\mathbb{P}\mathbb{P}f_0(980)}, g''_{\mathbb{P}\mathbb{P}f_0(980)}) = (0.788, 4.0)$, $(g'_{\mathbb{P}\mathbb{P}f_0(1500)}, g''_{\mathbb{P}\mathbb{P}f_0(1500)}) = (1.22, 6.0)$, and $(g'_{\mathbb{P}\mathbb{P}f_0(1370)}, g''_{\mathbb{P}\mathbb{P}f_0(1370)}) = (0.81, 0)$.

In Fig. 3 we show the distribution in azimuthal angle ϕ_{pp} between the outgoing protons for the central exclusive production of the $f_0(1710)$ meson at $\sqrt{s} = 29.1$ GeV with the data measured by the WA102 collaboration in [17]. Similarly as for the $f_0(980)$ and $f_0(1500)$ mesons (see Figs. 5 and 6 in [27], respectively) also for the $f_0(1710)$ meson both (l, S) contributions are necessary to describe the ϕ_{pp} distribution accurately. For the $f_0(1710)$ we obtain the coupling constants as $(g'_{\mathbb{P}\mathbb{P}f_0(1710)}, g''_{\mathbb{P}\mathbb{P}f_0(1710)}) = (0.45, 2.6)$.

The scalar-meson propagator in (3.32) is parametrized as

$$i\Delta^{(f_0)}(p_{34}) = \frac{i}{p_{34}^2 - m_{f_0}^2 + im_{f_0}\Gamma_{f_0}} \quad (3.36)$$

with a constant decay width.

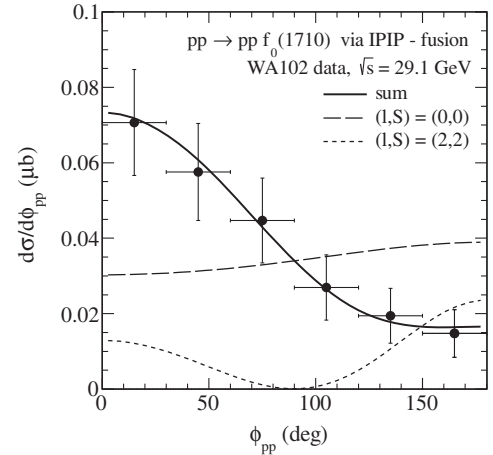


FIG. 3. The distribution in azimuthal angle ϕ_{pp} between the outgoing protons for central exclusive production of the $f_0(1710)$ meson by the fusion of two tensor pomerons at $\sqrt{s} = 29.1$ GeV. The experimental data points from [12] have been normalized to the total cross section $\sigma = 245$ nb from [17]. Plotted is the cross section $d\sigma/d\phi_{pp}$ for $0 < \phi_{pp} < \pi$. We show the individual contributions to the cross section with $(l, S) = (0, 0)$ (the long-dashed line), $(l, S) = (2, 2)$ (the short-dashed line), and their coherent sum (the solid line).

For the $f_0 KK$ vertex we have ($M_0 \equiv 1$ GeV)

$$i\Gamma^{(f_0 KK)}(p_3, p_4) = ig_{f_0 K^+ K^-} M_0 F^{(f_0 KK)}(p_{34}^2), \quad (3.37)$$

where the dimensionless coupling constant $g_{f_0 K^+ K^-}$ is related to the partial decay width of the f_0 meson (for an ‘‘on-shell’’ f_0 state $p_{34}^2 = m_{f_0}^2$)

$$\Gamma(f_0 \rightarrow K^+ K^-) = \frac{M_0^2}{16\pi m_{f_0}} |g_{f_0 K^+ K^-}|^2 \left(1 - \frac{4m_K^2}{m_{f_0}^2}\right)^{1/2}. \quad (3.38)$$

The analogous relation for $f_0 \rightarrow \pi^+ \pi^-$ reads

$$\Gamma(f_0 \rightarrow \pi^+ \pi^-) = \frac{M_0^2}{16\pi m_{f_0}} |g_{f_0 \pi^+ \pi^-}|^2 \left(1 - \frac{4m_\pi^2}{m_{f_0}^2}\right)^{1/2}. \quad (3.39)$$

In (3.37) we assume that $F^{(f_0 KK)}(p_{34}^2)$ has the same form as $F^{(\mathbb{P}\mathbb{P}f_0)}(p_{34}^2)$, see (3.35).

In order to estimate the coupling constants $g_{f_0 K^+ K^-}$ for the various f_0 states from (3.38) we need data for the partial decay rates $\Gamma(f_0 \rightarrow K^+ K^-)$. Since the Particle Data Group [44] does not give these decay rates explicitly we shall estimate them in the following using the available information.

The f_0 states have isospin $I = 0$. Assuming isospin invariance in the decays we get

$$\Gamma(f_0 \rightarrow K^+ K^-) = \Gamma(f_0 \rightarrow K^0 \bar{K}^0) = \frac{1}{2} \Gamma(f_0 \rightarrow K \bar{K}), \quad (3.40)$$

$$\Gamma(f_0 \rightarrow \pi^+ \pi^-) = 2\Gamma(f_0 \rightarrow \pi^0 \pi^0) = \frac{2}{3} \Gamma(f_0 \rightarrow \pi \pi). \quad (3.41)$$

Let us now consider the various f_0 states in turn. The $f_0(980)$ has only the $\pi\pi$, $K\bar{K}$ and the electromagnetic $\gamma\gamma$ decays. Therefore we have, to very good approximation, for the total decay rate

$$\Gamma_{f_0(980)} = \Gamma(f_0(980) \rightarrow \pi\pi) + \Gamma(f_0(980) \rightarrow K\bar{K}). \quad (3.42)$$

In [49] the ratio

$$\Gamma(f_0(980) \rightarrow K^+ K^-) / \Gamma(f_0(980) \rightarrow \pi^+ \pi^-) = 0.69 \pm 0.32 \quad (3.43)$$

was found from the B meson decays. To obtain $g_{f_0(980) K^+ K^-}$ we assume the approximate relation³

³We cannot use formula (3.38) for the $f_0(980) \rightarrow K^+ K^-$ decay as the threshold for the decay is above the $f_0(980)$ resonance position.

$$\sigma(f_0(980) \rightarrow K^+ K^-) / \sigma(f_0(980) \rightarrow \pi^+ \pi^-) = 0.69 \pm 0.32, \quad (3.44)$$

where $\sigma(f_0(980) \rightarrow \pi^+ \pi^-, K^+ K^-)$ are the integrated cross sections for the $pp \rightarrow pp(f_0(980) \rightarrow \pi^+ \pi^-, K^+ K^-)$ processes via the $\mathbb{P}\mathbb{P}$ fusion at $\sqrt{s} = 13$ TeV. We get from (3.40)–(3.44), and with $m_{f_0(980)} = 980$ MeV, $\Gamma_{f_0(980)} = 50$ MeV, assuming $g_{f_0(980) K^+ K^-} > 0$ and $g_{f_0(980) \pi^+ \pi^-} > 0$,

$$g_{f_0(980) K^+ K^-} = 2.88_{-0.77}^{+0.60}, \quad (3.45)$$

$$g_{f_0(980) \pi^+ \pi^-} = 0.95_{-0.09}^{+0.13}. \quad (3.46)$$

The error bars in (3.45) were obtained using only error bars in (3.44). Uncertainties of the rather poorly known $\Gamma_{f_0(980)}$ are similar.

For the $f_0(1370)$ meson we take the following input:

$$m_{f_0(1370)} = 1370 \text{ MeV}, \quad \Gamma_{f_0(1370)} = 350 \text{ MeV}, \quad (3.47)$$

from [44], and

$$\begin{aligned} \Gamma(f_0(1370) \rightarrow K\bar{K}) / \Gamma_{f_0(1370)} &= 0.35 \pm 0.13, \\ \Gamma(f_0(1370) \rightarrow \pi\pi) / \Gamma_{f_0(1370)} &= 0.26 \pm 0.09, \end{aligned} \quad (3.48)$$

from [50]. From (3.40) and (3.42) we get then, assuming again $g_{f_0(1370) K^+ K^-} > 0$ and $g_{f_0(1370) \pi^+ \pi^-} > 0$,

$$g_{f_0(1370) K^+ K^-} = 2.47, \quad (3.49)$$

$$g_{f_0(1370) \pi^+ \pi^-} = 2.07. \quad (3.50)$$

For the $f_0(1500)$ we have from [44]

$$m_{f_0(1500)} = 1504 \text{ MeV},$$

$$\Gamma_{f_0(1500)} = 109 \text{ MeV},$$

$$\begin{aligned} \Gamma(f_0(1500) \rightarrow K\bar{K}) / \Gamma_{f_0(1500)} &= 0.086 \pm 0.010, \\ \Gamma(f_0(1500) \rightarrow \pi\pi) / \Gamma_{f_0(1500)} &= 0.349 \pm 0.023. \end{aligned} \quad (3.51)$$

With (3.40) and (3.41) we get, assuming positive coupling constants

$$g_{f_0(1500) K^+ K^-} = 0.69, \quad (3.52)$$

$$g_{f_0(1500) \pi^+ \pi^-} = 1.40. \quad (3.53)$$

For the $f_0(1710)$, finally, we have from [44]

$$m_{f_0(1710)} = 1723 \text{ MeV}, \quad \Gamma_{f_0(1710)} = 139 \text{ MeV}, \quad (3.54)$$

and from [51]

$$\Gamma(f_0(1710) \rightarrow K\bar{K})/\Gamma_{f_0(1710)} = 0.36 \pm 0.12, \quad (3.55)$$

$$\Gamma(f_0(1710) \rightarrow \pi\pi)/\Gamma(f_0(1710) \rightarrow K\bar{K}) = 0.32 \pm 0.14. \quad (3.56)$$

The ratio (3.56) is consistent with $0.41_{-0.17}^{+0.11}$ from [52] and with $0.31_{-0.03}^{+0.05}$ from [53] within the errors. This gives, for positive couplings, from (3.40)–(3.41)

$$g_{f_0(1710)K^+K^-} = 2.36, \quad (3.57)$$

$$g_{f_0(1710)\pi^+\pi^-} = 1.40. \quad (3.58)$$

C. $f_2(1270)$ and $f_2'(1525)$ mesons central production

For diffractive K^+K^- production through the s -channel f_2 -meson exchange the amplitude is more complicated to treat. The $f_2(1270)$ and $f_2'(1525)$ mesons could be considered as potential candidates. The amplitude for the $\mathbb{P}\mathbb{P}$ fusion is given by

$$\begin{aligned} \mathcal{M}_{\lambda_a\lambda_b \rightarrow \lambda_1\lambda_2 K^+K^-}^{(\mathbb{P}\mathbb{P} \rightarrow f_2 \rightarrow K^+K^-)} &= (-i)\bar{u}(p_1, \lambda_1) i\Gamma_{\mu_1\nu_1}^{(\mathbb{P}\mathbb{P}\mathbb{P})}(p_1, p_a) u(p_a, \lambda_a) \\ &\times i\Delta^{(\mathbb{P})\mu_1\nu_1, \alpha_1\beta_1}(s_1, t_1) \\ &\times i\Gamma_{\alpha_1\beta_1, \alpha_2\beta_2, \rho\sigma}^{(\mathbb{P}\mathbb{P}f_2)}(q_1, q_2) i\Delta^{(f_2)\rho\sigma, \alpha\beta}(p_{34}) \\ &\times i\Gamma_{\alpha\beta}^{(f_2 KK)}(p_3, p_4) i\Delta^{(\mathbb{P})\alpha_2\beta_2, \mu_2\nu_2}(s_2, t_2) \\ &\times \bar{u}(p_2, \lambda_2) i\Gamma_{\mu_2\nu_2}^{(\mathbb{P}\mathbb{P}\mathbb{P})}(p_2, p_b) u(p_b, \lambda_b). \end{aligned} \quad (3.59)$$

The $\mathbb{P}\mathbb{P}f_2$ vertex can be written as

$$\begin{aligned} i\Gamma_{\mu\nu, \kappa\lambda, \rho\sigma}^{(\mathbb{P}\mathbb{P}f_2)}(q_1, q_2) &= \left(i\Gamma_{\mu\nu, \kappa\lambda, \rho\sigma}^{(\mathbb{P}\mathbb{P}f_2)(1)} \Big|_{\text{bare}} \right. \\ &+ \sum_{j=2}^7 i\Gamma_{\mu\nu, \kappa\lambda, \rho\sigma}^{(\mathbb{P}\mathbb{P}f_2)(j)}(q_1, q_2) \Big|_{\text{bare}} \left. \right) \\ &\times \tilde{F}^{(\mathbb{P}\mathbb{P}f_2)}(q_1^2, q_2^2, p_{34}^2). \end{aligned} \quad (3.60)$$

A possible choice for the $i\Gamma_{\mu\nu, \kappa\lambda, \rho\sigma}^{(\mathbb{P}\mathbb{P}f_2)(j)} \Big|_{\text{bare}}$ terms $j = 1, \dots, 7$ is given in Appendix A of [28]. In [28] we found that the $j = 2$ coupling for $g_{\mathbb{P}\mathbb{P}f_2(1270)}^{(2)} = 9.0$ is optimal to describe the main characteristics measured in the WA102 and ISR experiments and by the CDF collaboration [20] including e.g. a gap survival factor $\langle S^2 \rangle = 0.1$ for the CDF.

The $f_2(1270)$ and $f_2'(1525)$ have similar ϕ_{pp} and dP_t dependences [12]. dP_t is the so-called ‘‘glueball-filter variable’’ [54] defined by the difference of the transverse momentum vectors of the outgoing protons in (2.1)

$$dP_t = q_{t,1} - q_{t,2} = p_{t,2} - p_{t,1}, \quad dP_t = |dP_t|. \quad (3.61)$$

It has been observed in Ref. [9] that all the undisputed $q\bar{q}$ states (i.e. η , η' , $f_1(1285)$ etc.) are suppressed when $dP_t \rightarrow 0$, whereas the glueball candidates, e.g. $f_0(1500)$, survive. As can be seen in Refs. [9,12] the $f_2(1270)$ and $f_2'(1525)$ states have larger dP_t and their cross sections peak at $\phi_{pp} = \pi$ in contrast to the ‘‘enigmatic’’ $f_0(980)$, $f_0(1500)$ and $f_0(1710)$ states. Note, that at $\sqrt{s} = 29.1$ GeV the experimental cross section for the production of the $f_2(1270)$ meson, whose production has been found to be consistent with double Pomeron/Reggeon exchange, is more than 48 times greater than the cross section of the $f_2'(1525)$ meson [17]. For the $f_2'(1525)$ we assume also only the $j = 2$ coupling with $g_{\mathbb{P}\mathbb{P}f_2'(1525)}^{(2)} = 2.0$ fixed to the experimental total cross section from [17]. With this we roughly reproduced the shapes of the differential distributions of the WA102 data [12]. In the future the corresponding $\mathbb{P}\mathbb{P}f_2$ coupling constants could be adjusted by comparison with precise experimental data.

In (3.60) $\tilde{F}^{(\mathbb{P}\mathbb{P}f_2)}$ is a form factor for which we take

$$\tilde{F}^{(\mathbb{P}\mathbb{P}f_2)}(q_1^2, q_2^2, p_{34}^2) = F_M(q_1^2) F_M(q_2^2) F^{(\mathbb{P}\mathbb{P}f_2)}(p_{34}^2), \quad (3.62)$$

$$\begin{aligned} F^{(\mathbb{P}\mathbb{P}f_2)}(p_{34}^2) &= \exp\left(\frac{-(p_{34}^2 - m_{f_2}^2)^2}{\Lambda_{f_2}^4}\right), \\ \Lambda_{f_2} &= 1 \text{ GeV}. \end{aligned} \quad (3.63)$$

Here, for qualitative calculations only, one may use the tensor-meson propagator with the simple Breit-Wigner form

$$\begin{aligned} i\Delta_{\mu\nu, \kappa\lambda}^{(f_2)}(p_{34}) &= \frac{i}{p_{34}^2 - m_{f_2}^2 + im_{f_2}\Gamma_{f_2}} \\ &\times \left[\frac{1}{2}(\hat{g}_{\mu\kappa}\hat{g}_{\nu\lambda} + \hat{g}_{\mu\lambda}\hat{g}_{\nu\kappa}) - \frac{1}{3}\hat{g}_{\mu\nu}\hat{g}_{\kappa\lambda} \right], \end{aligned} \quad (3.64)$$

where $\hat{g}_{\mu\nu} = -g_{\mu\nu} + p_{34\mu}p_{34\nu}/p_{34}^2$. In (3.64) Γ_{f_2} is the total decay width of the f_2 resonance and m_{f_2} its mass.

The f_2KK vertex can be written as (see Eq. (3.37) of [24] for the analogous $f_2\pi\pi$ vertex)

$$\begin{aligned} i\Gamma_{\mu\nu}^{(f_2 KK)}(p_3, p_4) &= -i\frac{g_{f_2 K^+K^-}}{2M_0} \left[(p_3 - p_4)_\mu (p_3 - p_4)_\nu \right. \\ &\quad \left. - \frac{1}{4}g_{\mu\nu}(p_3 - p_4)^2 \right] F^{(f_2 KK)}(p_{34}^2), \end{aligned} \quad (3.65)$$

where $g_{f_2 K^+K^-}$ can be obtained from the corresponding partial decay width. We assume that

$$F^{(f_2 KK)}(p_{34}^2) = F^{(\mathbb{P}\mathbb{P}f_2)}(p_{34}^2) = \exp\left(\frac{-(p_{34}^2 - m_{f_2}^2)^2}{\Lambda_{f_2}^4}\right),$$

$$\Lambda_{f_2} = 1 \text{ GeV}. \quad (3.66)$$

In analogy to the $f_2 \rightarrow \pi\pi$ decay, treated in Sec. 5.1 of [24], we can write

$$\Gamma(f_2 \rightarrow K^+ K^-) = \frac{m_{f_2}}{480\pi} |g_{f_2 K^+ K^-}|^2 \left(\frac{m_{f_2}}{M_0}\right)^2 \left(1 - \frac{4m_K^2}{m_{f_2}^2}\right)^{5/2}. \quad (3.67)$$

We assume further that isospin symmetry holds, that is,

$$\Gamma(f_2 \rightarrow K^+ K^-) = \frac{1}{2} \Gamma(f_2 \rightarrow K \bar{K}). \quad (3.68)$$

With $\Gamma(f_2 \rightarrow K \bar{K})/\Gamma_{f_2}$ from [44] (see Table I) we get, assuming $g_{f_2 K^+ K^-} > 0$,

$$g_{f_2(1270)K^+K^-} = 5.54, \quad (3.69)$$

$$g_{f_2'(1525)K^+K^-} = 7.32. \quad (3.70)$$

For the $\pi^+\pi^-$ decay channel, based on (5.6) of [24] and the numerical values from Table I, we have

$$g_{f_2(1270)\pi^+\pi^-} = 9.28, \quad (3.71)$$

$$g_{f_2'(1525)\pi^+\pi^-} = 0.43. \quad (3.72)$$

IV. PHOTOPRODUCTION CONTRIBUTIONS

For the ϕ resonance production we consider the diagrams shown in Fig. 4. In these diagrams all vertices and propagators will be taken here according to Ref. [24]. The diagrams to be considered for the nonresonant (Drell-Söding) contribution are shown in Fig. 5. In the following we collect formulas for the amplitudes for the $pp \rightarrow ppK^+K^-$ reaction within the tensor-Pomeron approach [24].

A. K^+K^- continuum central production

The amplitude for photoproduction of the K^+K^- continuum can be written as the following sum:

$$\mathcal{M}_{pp \rightarrow ppK^+K^-}^{KK\text{-continuum}} = \mathcal{M}^{(\gamma\mathbb{P} \rightarrow K^+K^-)} + \mathcal{M}^{(\mathbb{P}\gamma \rightarrow K^+K^-)} + \mathcal{M}^{(\gamma\mathbb{R} \rightarrow K^+K^-)} + \mathcal{M}^{(\mathbb{R}\gamma \rightarrow K^+K^-)}. \quad (4.1)$$

The $\gamma\mathbb{P}$ -exchange amplitude can be written as the sum:

$$\mathcal{M}^{(\gamma\mathbb{P} \rightarrow K^+K^-)} = \mathcal{M}_{\lambda_a \lambda_b \rightarrow \lambda_1 \lambda_2 K^+ K^-}^{(a)} + \mathcal{M}_{\lambda_a \lambda_b \rightarrow \lambda_1 \lambda_2 K^+ K^-}^{(b)} + \mathcal{M}_{\lambda_a \lambda_b \rightarrow \lambda_1 \lambda_2 K^+ K^-}^{(c)}, \quad (4.2)$$

where

$$\begin{aligned} \mathcal{M}_{\lambda_a \lambda_b \rightarrow \lambda_1 \lambda_2 K^+ K^-}^{(a)} &= (-i)\bar{u}(p_1, \lambda_1) i\Gamma_{\mu}^{(\gamma PP)}(p_1, p_a) u(p_a, \lambda_a) i\Delta^{(\gamma)\mu\nu}(q_1) i\Gamma_{\nu}^{(\gamma KK)}(p_t, -p_3) \\ &\quad \times i\Delta^{(K)}(p_t) i\Gamma_{\alpha\beta}^{(\mathbb{P}KK)}(p_4, p_t) i\Delta^{(\mathbb{P})\alpha\beta, \delta\eta}(s_2, t_2) \bar{u}(p_2, \lambda_2) i\Gamma_{\delta\eta}^{(\mathbb{P}PP)}(p_2, p_b) u(p_b, \lambda_b), \end{aligned} \quad (4.3)$$

$$\begin{aligned} \mathcal{M}_{\lambda_a \lambda_b \rightarrow \lambda_1 \lambda_2 K^+ K^-}^{(b)} &= (-i)\bar{u}(p_1, \lambda_1) i\Gamma_{\mu}^{(\gamma PP)}(p_1, p_a) u(p_a, \lambda_a) i\Delta^{(\gamma)\mu\nu}(q_1) i\Gamma_{\nu}^{(\gamma KK)}(p_4, p_u) \\ &\quad \times i\Delta^{(K)}(p_u) i\Gamma_{\alpha\beta}^{(\mathbb{P}KK)}(p_u, -p_3) i\Delta^{(\mathbb{P})\alpha\beta, \delta\eta}(s_2, t_2) \bar{u}(p_2, \lambda_2) i\Gamma_{\delta\eta}^{(\mathbb{P}PP)}(p_2, p_b) u(p_b, \lambda_b), \end{aligned} \quad (4.4)$$

$$\begin{aligned} \mathcal{M}_{\lambda_a \lambda_b \rightarrow \lambda_1 \lambda_2 K^+ K^-}^{(c)} &= (-i)\bar{u}(p_1, \lambda_1) i\Gamma_{\mu}^{(\gamma PP)}(p_1, p_a) u(p_a, \lambda_a) i\Delta^{(\gamma)\mu\nu}(q_1) i\Gamma_{\nu, \alpha\beta}^{(\mathbb{P}\gamma KK)}(q_1, p_4, -p_3) \\ &\quad \times i\Delta^{(\mathbb{P})\alpha\beta, \delta\eta}(s_2, t_2) \bar{u}(p_2, \lambda_2) i\Gamma_{\delta\eta}^{(\mathbb{P}PP)}(p_2, p_b) u(p_b, \lambda_b). \end{aligned} \quad (4.5)$$

Here the γ and \mathbb{P} propagators and the γPP , $\mathbb{P}PP$ vertices are given in Sec. 3 of [24]. The K propagator is standard and given after (3.4) above. The γKK , $\mathbb{P}KK$ and $\mathbb{P}\gamma KK$ vertices are as the corresponding vertices for pions, see Appendix B of [30], but with $\beta_{\mathbb{P}\pi\pi}$ replaced by $\beta_{\mathbb{P}KK}$ (3.30).

In order to assure gauge invariance and ‘‘proper’’ cancellations among the three terms (4.3) to (4.5) we have introduced, somewhat arbitrarily, one common energy dependence on s_2 defined as:

$$s_2 = (p_b + q_1)^2 = (p_2 + p_{34})^2 \quad (4.6)$$

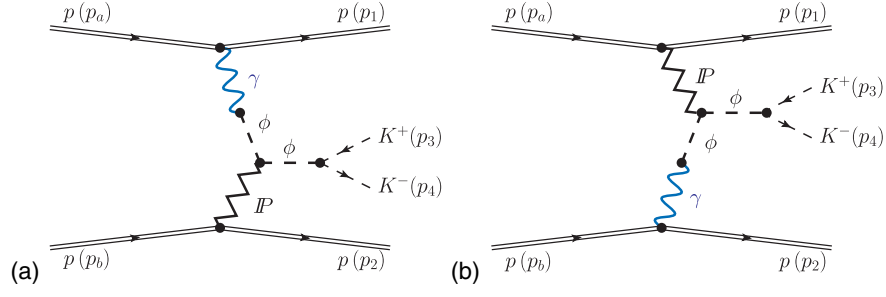


FIG. 4. The central exclusive ϕ meson production and its subsequent decay into P -wave K^+K^- in proton-proton collisions.

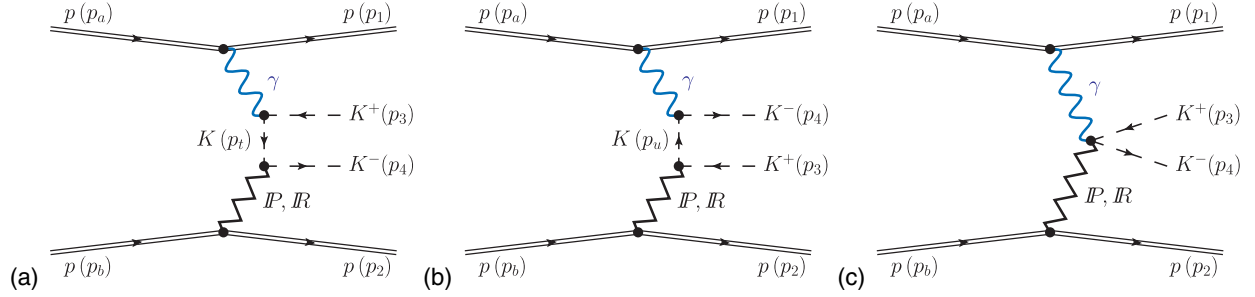


FIG. 5. The diagrams for photon-induced central exclusive continuum K^+K^- production in proton-proton collisions. There are also 3 additional diagrams with the role of $(p(p_a), p(p_1))$ and $(p(p_b), p(p_2))$ exchanged.

for the Pomeron propagator in all three diagrams. Gauge invariance requires

$$\{\mathcal{M}^{(a)} + \mathcal{M}^{(b)} + \mathcal{M}^{(c)}\}_{p_1+p_a \rightarrow q_1} = 0. \quad (4.7)$$

This is satisfied as we see easily by replacing in (4.3)–(4.5) $\Gamma_\mu^{(\gamma PP)}(p_1, p_a)$ by $q_{1\mu}$. The formulas (4.3)–(4.5) do not include hadronic form factors for the inner subprocess $\gamma P \rightarrow K^+K^-$. A possible way to include form factors for the inner subprocesses is to multiply the amplitude obtained from (4.3) to (4.5) with a common factor, see [29,55–57],

$$\mathcal{M}^{(\gamma P \rightarrow K^+K^-)} = (\mathcal{M}^{(a)} + \mathcal{M}^{(b)} + \mathcal{M}^{(c)})F(p_t^2, p_u^2, p_{34}^2). \quad (4.8)$$

A common form factor for all three diagrams is chosen in order to maintain gauge invariance, and a convenient form is given in [58]

$$F(p_t^2, p_u^2, p_{34}^2) = \frac{[F(p_t^2)]^2 + [F(p_u^2)]^2}{1 + [\tilde{F}(p_{34}^2)]^2}, \quad (4.9)$$

with the exponential parametrizations

$$F(p_t^2) = \exp\left(\frac{p_t^2 - m_K^2}{\Lambda_K^2}\right), \quad (4.10)$$

$$F(p_u^2) = \exp\left(\frac{p_u^2 - m_K^2}{\Lambda_K^2}\right), \quad (4.11)$$

$$\tilde{F}(p_{34}^2) = \exp\left(\frac{-(p_{34}^2 - 4m_K^2)}{\Lambda_K^2}\right). \quad (4.12)$$

The parameter Λ_K should be fitted to the experimental data. We expect it in the range of 0.8 to 1 GeV.

For the $\mathbb{P}\gamma$ -exchange the amplitude has the same structure with $p(p_a), p(p_1) \leftrightarrow p(p_b), p(p_2)$, $t_1 \leftrightarrow t_2$ and $s_2 \leftrightarrow s_1$. We shall consider also contributions involving nonleading Reggeons. For the $f_{2\mathbb{R}}$ exchange the formulae have the same tensorial structure as for Pomeron exchange and are obtained from (4.3) to (4.5) with the corresponding effective $f_{2\mathbb{R}}pp$, $f_{2\mathbb{R}}KK$ and $f_{2\mathbb{R}}\gamma KK$ vertices and the $f_{2\mathbb{R}}$ reggeon propagator; see [24,30]. Analogous statements hold for the case for the $a_{2\mathbb{R}}$ Reggeon exchange. The relevant Reggeon-kaon coupling constants are given in Eq. (3.31). The contributions involving $C = -1$ Reggeon exchanges are different. We recall that $\mathbb{R}_- = \omega_{\mathbb{R}}, \rho_{\mathbb{R}}$ exchanges are treated as effective vector exchanges in our model; see Sec. 3 of [24]. The vertex for $\rho_{\mathbb{R}}\gamma KK$ is in analogy to the vertex $\rho_{\mathbb{R}}\gamma\pi\pi$ given in (B.81) of [30]. The $\omega_{\mathbb{R}}$ exchange is treated in a similar way.

B. Photoproduction of ϕ meson

Since the proton contains no valence s quarks we shall assume that the amplitude for the $\gamma p \rightarrow \phi p$ reaction at high energies includes only the Pomeron exchange contribution.

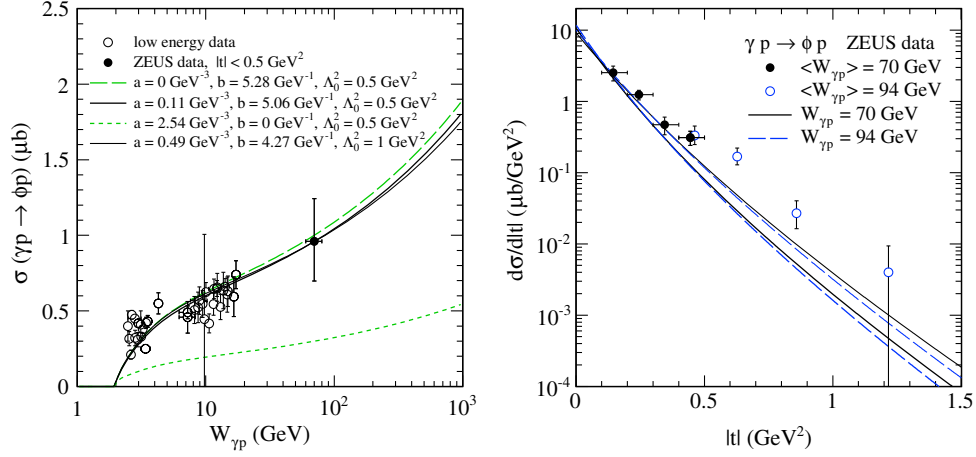


FIG. 6. Left panel: The elastic ϕ photoproduction cross section as a function of the center-of-mass energy $W_{\gamma p}$. Our results are compared with the HERA data [60] (solid mark) and with a compilation of low energy data from [61–68] (open circles). Right panel: The differential cross section $d\sigma/d|t|$ for the $\gamma p \rightarrow \phi p$ process. The ZEUS data at low $|t|$ (at γp average center-of-mass energy $\langle\sqrt{s}\rangle = 70$ GeV and the squared photon virtuality $Q^2 = 0$ GeV 2 , solid marks, [60]) and at higher $|t|$ (at $\langle\sqrt{s}\rangle = 94$ GeV and $Q^2 < 0.01$ GeV 2 , open circles, [69]) are shown. The black solid lines represent the results for $\sqrt{s} = 70$ GeV, while the blue dashed lines represent the results for $\sqrt{s} = 94$ GeV. The thick lines correspond to results with $\Lambda_0^2 = 0.5$ GeV 2 , $a_{\mathbb{P}\phi\phi} = 0.11$ GeV $^{-3}$, and $b_{\mathbb{P}\phi\phi} = 5.06$ GeV $^{-1}$. The thin lines correspond to results with $\Lambda_0^2 = 1$ GeV 2 , $a_{\mathbb{P}\phi\phi} = 0.49$ GeV $^{-3}$, and $b_{\mathbb{P}\phi\phi} = 4.27$ GeV $^{-1}$.

In contrast, in the amplitudes for the $\gamma p \rightarrow \rho^0 p$ reaction [29,30] and for the $\gamma p \rightarrow \omega p$ reaction [59] also Reggeon exchanges play an important role.

The amplitude for the $\gamma p \rightarrow \phi p$ reaction with the tensor-Pomeron exchange can be written in complete analogy to $\gamma p \rightarrow \rho^0 p$ (see [29,30]) as follows

$$\begin{aligned}
 & \langle \phi(p_\phi, \lambda_\phi), p(p_2, \lambda_2) | T | \gamma(q, \lambda_\gamma), p(p_b, \lambda_b) \rangle \\
 & \equiv \mathcal{M}_{\lambda_\gamma \lambda_b \rightarrow \lambda_\phi \lambda_2}(s, t) \\
 & = (-i)(\epsilon^{(\phi)\mu})^* i \Gamma_{\mu\nu\alpha\beta}^{(\mathbb{P}\phi\phi)}(p_\phi, q) \\
 & \quad \times i \Delta^{(\phi)\nu\kappa}(q) i \Gamma_{\kappa\sigma}^{(\gamma\rightarrow\phi)}(q) \epsilon^{(\gamma)\sigma} i \Delta^{(\mathbb{P})\alpha\beta, \delta\eta}(s, t) \\
 & \quad \times \bar{u}(p_2, \lambda_2) i \Gamma_{\delta\eta}^{(\mathbb{P}pp)}(p_2, p_b) u(p_b, \lambda_b), \quad (4.13)
 \end{aligned}$$

where p_b , p_2 and λ_b , $\lambda_2 = \pm \frac{1}{2}$ denote the four-momenta and helicities of the ingoing and outgoing protons, $\epsilon^{(\gamma)}$ and $\epsilon^{(\phi)}$ are the polarization vectors for photon and ϕ meson with the four-momenta q , p_ϕ and helicities $\lambda_\gamma = \pm 1$, $\lambda_\phi = \pm 1, 0$, respectively. We use standard kinematic variables

$$\begin{aligned}
 s & = W_{\gamma p}^2 = (p_b + q)^2 = (p_2 + p_\phi)^2, \\
 t & = (p_2 - p_b)^2 = (p_\phi - q)^2. \quad (4.14)
 \end{aligned}$$

In (4.13) the ϕ propagator is of the same structure as for ρ^0 and ω in (3.2) of [24]. Our ansatz for the $\mathbb{P}\phi\phi$ vertex follows the one for the $\mathbb{P}\rho\rho$ in (3.47) of [24].

In the high-energy small-angle approximation we get, using (D.19) in Appendix D of [27],

$$\begin{aligned}
 \mathcal{M}_{\lambda_\gamma \lambda_b \rightarrow \lambda_\phi \lambda_2}(s, t) & \cong i e \frac{m_\phi^2}{\gamma_\phi} \Delta_T^{(\phi)}(0) (\epsilon^{(\phi)\mu})^* \epsilon^{(\gamma)\nu} \\
 & \quad \times [2a_{\mathbb{P}\phi\phi} \Gamma_{\mu\nu\kappa\lambda}^{(0)}(p_\phi, -q) \\
 & \quad - b_{\mathbb{P}\phi\phi} \Gamma_{\mu\nu\kappa\lambda}^{(2)}(p_\phi, -q)] \\
 & \quad \times 3\beta_{\mathbb{P}NN} \frac{1}{2s} (-i s \alpha'_{\mathbb{P}})^{\alpha_{\mathbb{P}}(t)-1} (p_2 + p_b)^\kappa \\
 & \quad \times (p_2 + p_b)^\lambda \delta_{\lambda_2 \lambda_b} F_1(t) F_M(t), \quad (4.15)
 \end{aligned}$$

where the explicit tensorial functions $\Gamma_{\mu\nu\kappa\lambda}^{(i)}(p_\phi, -q)$, $i = 0, 2$, are given in Ref. [24], formulas (3.18) and (3.19), respectively. In Eq. (4.15) $4\pi/\gamma_\phi^2 = 0.0716$, $(\Delta_T^{(\phi)}(0))^{-1} = -m_\phi^2$. The form factors $F_1(t)$ and $F_M(t)$ are chosen in (4.15) as the electromagnetic form factors (3.10) only for simplicity. Here, it seems reasonable to assume rather $\Lambda_0^2 \approx m_\phi^2$ than $\Lambda_0^2 = 0.5$ GeV 2 from (3.10). This will be discussed in Fig. 6. Alternatively, we can take a common form factor

$$F_{\phi p}^{(\mathbb{P})}(t) = \exp(B_{\phi p}^{(\mathbb{P})} t/2). \quad (4.16)$$

with the slope parameter $B_{\phi p}^{(\mathbb{P})}$ obtained from comparison to the experimental data.

In order to get estimates for the $\mathbb{P}\phi\phi$ coupling constants $a_{\mathbb{P}\phi\phi}$ and $b_{\mathbb{P}\phi\phi}$ we make the assumption based on the additive quark model [70–74] (see also chapter II of [75]):

$$\sigma_{\text{tot}}(\phi(\epsilon^{(m)}), p) = \sigma_{\text{tot}}(K^+, p) + \sigma_{\text{tot}}(K^-, p) - \sigma_{\text{tot}}(\pi^-, p) \quad (4.17)$$

for transversely polarised ϕ mesons ($m = \pm 1$). In analogy to the ρp scattering discussed in Sec. 7.2 of [24] the total cross section for the ϕp scattering at high energies is obtained from (4.15) as

$$\begin{aligned} \sigma_{\text{tot}}(\phi(\epsilon^{(m)}), p) &= 3\beta_{\mathbb{P}NN} [2m_\phi^2 a_{\mathbb{P}\phi\phi} + (1 - \delta_{m,0}) b_{\mathbb{P}\phi\phi}] \\ &\times \cos \left[\frac{\pi}{2} (\alpha_{\mathbb{P}}(0) - 1) \right] (s\alpha'_{\mathbb{P}})^{\alpha_{\mathbb{P}}(0)-1}, \end{aligned} \quad (4.18)$$

$m = \pm 1, 0$. With the Pomeron parts of the Kp and πp total cross sections from (3.27) above and (7.6) of [24], respectively, we obtain from (4.17) and (4.18)

$$3\beta_{\mathbb{P}NN} (2m_\phi^2 a_{\mathbb{P}\phi\phi} + b_{\mathbb{P}\phi\phi}) = 12\beta_{\mathbb{P}NN} (2\beta_{\mathbb{P}KK} - \beta_{\mathbb{P}\pi\pi}). \quad (4.19)$$

From (4.19), (3.30) and $\beta_{\mathbb{P}\pi\pi} = 1.76 \text{ GeV}^{-1}$ we get

$$2m_\phi^2 a_{\mathbb{P}\phi\phi} + b_{\mathbb{P}\phi\phi} = 4(2\beta_{\mathbb{P}KK} - \beta_{\mathbb{P}\pi\pi}) = 5.28 \text{ GeV}^{-1}. \quad (4.20)$$

In the left panel of Fig. 6 we show the integrated cross section for the $\gamma p \rightarrow \phi p$ reaction, calculated from (4.13), as a function of the center-of-mass energy together with the experimental data. The experimental point at $W_{\gamma p} = 70 \text{ GeV}$ was obtained by extrapolating the differential cross section to $t = 0$ assuming a simple exponential t dependence and integrating over the range $|t| < 0.5 \text{ GeV}^2$ [60]. In our calculation we also integrate over the same t range. We see that our model calculation including only the Pomeron exchange describes the total cross section for the $\gamma p \rightarrow \phi p$ reaction fairly well.⁴

The right panel of Fig. 6 shows the differential cross section for elastic ϕ photoproduction. The calculations, performed for two energies, $W_{\gamma p} = 70 \text{ GeV}$ and 94 GeV , are compared with ZEUS data, [60,69], respectively. We show results for two parameters of the form factor $F_M(t)$, $\Lambda_0^2 = 0.5 \text{ GeV}^2$ and 1 GeV^2 , represented by the bottom lines and the top lines, respectively. We can see that the results for $\Lambda_0^2 = 1 \text{ GeV}^2$ with the relevant values of coupling constants a and b describe more accurately the slope of the t distribution.

C. $\phi(1020)$ meson central production

The ϕ photoproduction is dominated by diffractive scattering via Pomeron exchange. The amplitude for the

⁴At low energies there are other processes contributing, such as t -channel π^0 , η , σ meson exchanges; see [76,77]. Thus, the Pomeron exchange alone should not be expected to fit the low-energy data precisely. We refer the reader to [78,79] for measurements of the $\gamma p \rightarrow \phi p$ reaction near threshold.

$\gamma^{\mathbb{P}}$ -exchange, see diagram (a) in Fig. 4, reads as (3.5) of [29] with appropriate modifications:

$$\begin{aligned} \mathcal{M}_{\lambda_a \lambda_b \rightarrow \lambda_1 \lambda_2 K^+ K^-}^{(\gamma^{\mathbb{P}} \rightarrow \phi \rightarrow K^+ K^-)} &= (-i) \bar{u}(p_1, \lambda_1) i \Gamma_\mu^{(\gamma p p)}(p_1, p_a) u(p_a, \lambda_a) \\ &\times i \Delta^{(\gamma)\mu\sigma}(q_1) i \Gamma_{\sigma\nu}^{(\gamma \rightarrow \phi)}(q_1) i \Delta^{(\phi)\nu\rho_1}(q_1) \\ &\times i \Delta^{(\phi)\rho_2\kappa}(p_{34}) i \Gamma_\kappa^{(\phi K K)}(p_3, p_4) \\ &\times i \Gamma_{\rho_2 \rho_1 \alpha \beta}^{(\mathbb{P}\phi\phi)}(p_{34}, q_1) i \Delta^{(\mathbb{P})\alpha\beta,\delta\eta}(s_2, t_2) \\ &\times \bar{u}(p_2, \lambda_2) i \Gamma_{\delta\eta}^{(\mathbb{P} p p)}(p_2, p_b) u(p_b, \lambda_b). \end{aligned} \quad (4.21)$$

Here we use the ϕ propagator with the simple Breit-Wigner expression as defined in (3.7), (3.10) and (3.11) of [29] with

$$\Delta_T^{(\phi)}(s) = \frac{1}{s - m_\phi^2 + i\sqrt{s}\Gamma_\phi(s)}. \quad (4.22)$$

In (4.22) the running (energy-dependent) width is approximately parametrized as

$$\Gamma_\phi(s) = \Gamma_\phi \left(\frac{s - 4m_K^2}{m_\phi^2 - 4m_K^2} \right)^{3/2} \frac{m_\phi^2}{s} \theta(s - 4m_K^2). \quad (4.23)$$

A more accurate parametrization of $\Delta_T^{(\phi)}(s)$ and $\Gamma_\phi(s)$ must take into account also non- $K\bar{K}$ decay channels of the ϕ , in particular, the 3π decays which amount to $(15.32 \pm 0.32)\%$ of all decays, see [44]. For such a program one could use the methods explained for the ρ propagator in [80]; see also [24,30].

For the $\phi K K$ vertex we have

$$i \Gamma_\kappa^{(\phi K K)}(p_3, p_4) = -\frac{i}{2} g_{\phi K^+ K^-} (p_3 - p_4)_\kappa. \quad (4.24)$$

The $g_{\phi K^+ K^-}$ coupling constant can be determined from the partial decay width $\Gamma(\phi \rightarrow K^+ K^-)$,

$$\Gamma(\phi \rightarrow K^+ K^-) = \frac{1}{24\pi} \frac{p_K^3}{m_\phi^2} |g_{\phi K^+ K^-}|^2, \quad (4.25)$$

where $p_K = \sqrt{m_\phi^2/4 - m_K^2}$. With the parameters of Table I, assuming $g_{\phi K^+ K^-} > 0$, we get

$$g_{\phi K^+ K^-} = 8.92. \quad (4.26)$$

In the diagram of Fig. 4 at the $\mathbb{P}\phi\phi$ vertex the incoming ϕ is always off shell, the outgoing ϕ also may be away from the nominal ‘‘mass shell’’ $p_{34}^2 = m_\phi^2$. As suggested in [30], see (B.82) there, we insert, therefore, in the $\mathbb{P}\phi\phi$ vertex

extra form factors. A convenient form, given in (B.85) of [30] (see also (3.9) of [29]) is

$$\tilde{F}^{(\phi)}(k^2) = \left[1 + \frac{k^2(k^2 - m_\phi^2)}{\tilde{\Lambda}_\phi^4} \right]^{-\tilde{n}_\phi} \quad (4.27)$$

with $\tilde{\Lambda}_\phi$ a parameter close to 2 GeV and $\tilde{n}_\phi > 0$. In practical calculations we also include in (4.24) the form factor

$$F^{(\phi KK)}(p_{34}^2) = \exp\left(\frac{-(p_{34}^2 - m_\phi^2)^2}{\Lambda_\phi^4}\right),$$

$$\Lambda_\phi = 1 \text{ GeV}. \quad (4.28)$$

V. RESULTS

In this section we present results for integrated cross sections of the reaction $pp \rightarrow ppK^+K^-$ and dikaon invariant mass distributions. For convenience of the reader we collect in Table II the numerical values of default parameters of our model used in calculations. There are also the parameters of pomeron/reggeon-kaon couplings, see (3.30) and (3.31), not shown in Table II, obtained from fits to kaon-nucleon total cross-section data as discussed in Sec. III A. Our attempts to determine the parameters of pomeron-pomeron-meson couplings as far as possible from experimental data have been presented in Secs. III B and III C, and in Refs. [27,28]. Note that we take here somewhat smaller values of the Pomeron-Pomeron-meson coupling parameters than in our previous paper [27] because there they were fixed at the WA102 energy where we expect also large contributions to the cross sections from the Reggeon exchanges. We have checked for the central K^+K^- continuum contribution calculated at $\sqrt{s} = 13$ TeV and for three different cuts on pseudorapidities $|\eta_K| < 1$, $|\eta_K| < 2.5$, and $2 < \eta_K < 4.5$, that adding the exchange of secondary reggeons increases the cross section by 2.4%, 2.9%, and 6.5%, respectively. We expect a similar role of secondary Reggeons for production of resonances at $\sqrt{s} = 13$ TeV. For continuum K^+K^- photoproduction we find even less effect on the cross sections from secondary reggeons than for the purely diffractive production above. Recently, in Ref. [33], we also discussed the role of reggeons for the $pp \rightarrow ppp\bar{p}$ reaction.

Many of the parameters listed in Table II were obtained from fits to available data but they are still rather uncertain and some are only our educated guess. Clearly, it would be desirable to experimentally test our predictions obtained with our default parameters and then adjust these if necessary. Such an adjustment of the model parameters will be possible with high-energy experimental data for the purely exclusive reactions $pp \rightarrow pp\pi^+\pi^-$ and $pp \rightarrow ppK^+K^-$ which are expected to become available soon. The GENEX Monte Carlo generator [81] could be used in this context.

TABLE II. Some parameters of our model. The columns indicate the equation numbers where the parameter is defined and their numerical values used in the calculations.

Parameter for	Equation	Value
<i>Diffractive continuum</i>		
$\Lambda_{\text{off},M}$	(3.11)	0.7 GeV
Λ_0^2	(3.10); (3.34) of [24]	0.5 GeV ²
M_0	(3.13)–(3.16), (3.26) et seq.	1 GeV
M_-	(3.19), (3.26) et seq.; (6.63) of [24]	1.41 GeV
$f_0(980)$		
$g'_{\mathbb{P}\mathbb{P}f_0}$	(3.33) et seq.; (A.18) of [27]	0.53
$g''_{\mathbb{P}\mathbb{P}f_0}$	(3.33) et seq.; (A.20) of [27]	2.67
$g_{f_0K^+K^-}$	(3.38), (3.45)	3.48
Λ_{f_0}	(3.35)	1 GeV
$f_0(1500)$		
$g'_{\mathbb{P}\mathbb{P}f_0}$	(3.33) et seq.; (A.18) of [27]	0.35
$g''_{\mathbb{P}\mathbb{P}f_0}$	(3.33) et seq.; (A.20) of [27]	1.71
$g_{f_0K^+K^-}$	(3.38), (3.52)	0.69
Λ_{f_0}	(3.35)	1 GeV
$f_0(1710)$		
$g'_{\mathbb{P}\mathbb{P}f_0}$	(3.33) et seq.; (A.18) of [27]	0.23
$g''_{\mathbb{P}\mathbb{P}f_0}$	(3.33) et seq.; (A.20) of [27]	1.3
$g_{f_0K^+K^-}$	(3.38), (3.57)	2.36
Λ_{f_0}	(3.35)	1 GeV
$f_2(1270)$		
$g'_{\mathbb{P}\mathbb{P}f_2}$	(3.60) et seq.; (A.13) of [28]	9.0
$g_{f_2K^+K^-}$	(3.67), (3.69)	5.54
Λ_{f_2}	(3.66)	1 GeV
$f_2'(1525)$		
$g'_{\mathbb{P}\mathbb{P}f_2}$	(3.60) et seq.; (A.13) of [28]	2.0
$g_{f_2K^+K^-}$	(3.67), (3.70)	7.32
Λ_{f_2}	(3.66)	1 GeV
<i>Photoproduction continuum</i>		
Λ_K	(4.9)–(4.12)	1 GeV
$\phi(1020)$		
$a_{\mathbb{P}\phi\phi}$	(4.20) et seq.	0.49 GeV ⁻³
$b_{\mathbb{P}\phi\phi}$	(4.20) et seq.	4.27 GeV ⁻¹
Λ_0^2	(3.10)	1 GeV ²
$g_{\phi K^+K^-}$	(4.24)–(4.26)	8.92
$\tilde{\Lambda}_\phi$	(4.27); (3.9) of [29]	2 GeV
\tilde{n}_ϕ	(4.27); (3.9) of [29]	0.5
Λ_ϕ	(4.28)	1 GeV

In Fig. 7 we present the K^+K^- invariant mass distribution at $\sqrt{s} = 13$ TeV and $|\eta_K| < 1$. Here we take into account the non-resonant continuum, including both Pomeron and Reggeon exchanges, and the scalar $f_0(980)$ resonance created here only by the Pomeron-Pomeron fusion. We show results for different values of the relative phase $\phi_{f_0(980)}$ in the coupling constant (3.45) not known *a priori*

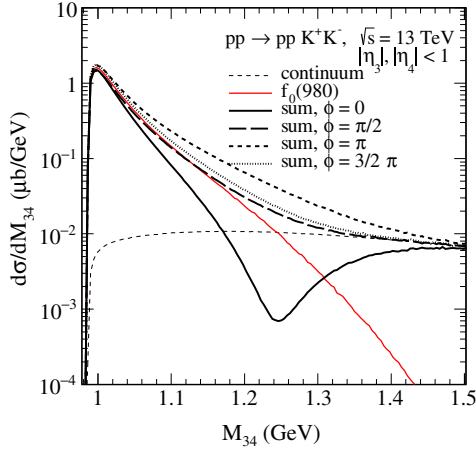


FIG. 7. Two-kaon invariant mass distribution for $pp \rightarrow ppK^+K^-$ at $\sqrt{s} = 13$ TeV and $|\eta_K| < 1$. Absorption effects were included here by the gap survival factor $\langle S^2 \rangle = 0.1$. Results for a coherent sum of non-resonant continuum and $f_0(980)$ meson for different values of the phase factor $\phi_{f_0(980)}$ in (5.1) are shown for illustration. The short-dashed line represents the nonresonant continuum contribution obtained for the monopole off-shell kaon form factors (3.11) with $\Lambda_{\text{off},M} = 0.7$ GeV. The red solid line represents the $f_0(980)$ resonant term.

$$g_{f_0(980)K^+K^-} \rightarrow g_{f_0(980)K^+K^-} e^{i\phi_{f_0(980)}}. \quad (5.1)$$

We can see that the complete result indicates a large interference effect of the continuum and the $f_0(980)$ terms. It should be recalled that the $f_0(980)$ resonance appears as a sharp drop around the 1 GeV region in the $\pi^+\pi^-$ mass

spectrum. The black solid line corresponds to the calculations with the phase used for $\pi^+\pi^-$ exclusive production. The phase for K^+K^- does not need to be the same as the production of $\pi\pi$ and $K\bar{K}$ systems may be a complicated coupled-channel effect not treated here explicitly. In some of the following figures we show predictions for two representative values for this phase, $\phi_{f_0(980)} = 0$ and $\pi/2$. We must leave it to the experiments to determine this phase from data.

As can be clearly seen from the left panel of Fig. 8 the resonance contributions generate a highly structured pattern. In the calculations we include the nonresonant continuum, and the dominant scalar $f_0(980)$, $f_0(1500)$, $f_0(1710)$, and tensor $f_2(1270)$, $f_2'(1525)$, resonances decaying into the K^+K^- pairs. In principle, there may also be a contribution from the broad scalar $f_0(1370)$ meson. The right panel of Fig. 8 shows the photoproduction contributions without and with some form factors included in the amplitudes. The narrow $\phi(1020)$ resonance is visible above the continuum term. It may in principle also be visible on top of the broader $f_0(980)$ resonance. This will be discussed in Fig. 10.

In Figs. 9 and 10 we show the invariant mass distributions for centrally produced $\pi^+\pi^-$ (the black lines) and K^+K^- (the blue lines) pairs imposing cuts on pseudorapidities and transverse momenta of produced particles that will be measured in the RHIC and LHC experiments. The $pp \rightarrow pp\pi^+\pi^-$ reaction was discussed within the tensor-pomeron model in [28]. The short-dashed lines represent the purely diffractive continuum term. The solid lines represent the coherent sum of the diffractive continuum,

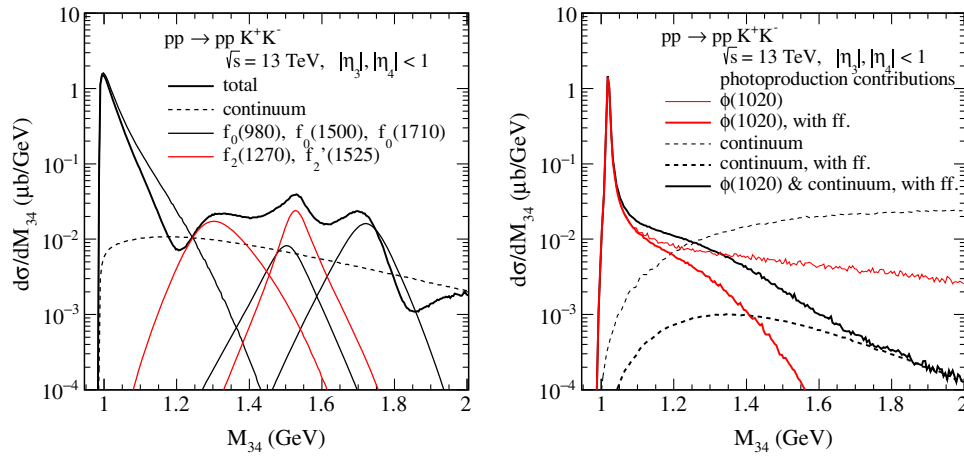


FIG. 8. Two-kaon invariant mass distributions for $pp \rightarrow ppK^+K^-$ at $\sqrt{s} = 13$ TeV and $|\eta_K| < 1$. The left panel shows the purely diffractive contributions and the right panel shows the diffractive photoproduction results. In the left panel the black line represents a coherent sum of nonresonant continuum, and $f_0(980)$, $f_0(1500)$, $f_0(1710)$, $f_2(1270)$ and $f_2'(1525)$ resonant terms. For the $f_0(980)$ resonant term we take $\phi_{f_0(980)} = 0$ in (5.1). The dashed line represents the nonresonant continuum contribution. The individual resonance contributions are shown for better understanding. In the right panel the photoproduction terms are shown without and with some form factors included in the amplitudes. The lower lines correspond to results for the $\phi(1020)$ photoproduction with form factor (4.28) and for the nonresonant term with form factors (4.9)–(4.12). Absorption effects have been included here by the gap survival factors $\langle S^2 \rangle = 0.1$ for the diffractive contributions and $\langle S^2 \rangle = 0.9$ for the photoproduction contributions.

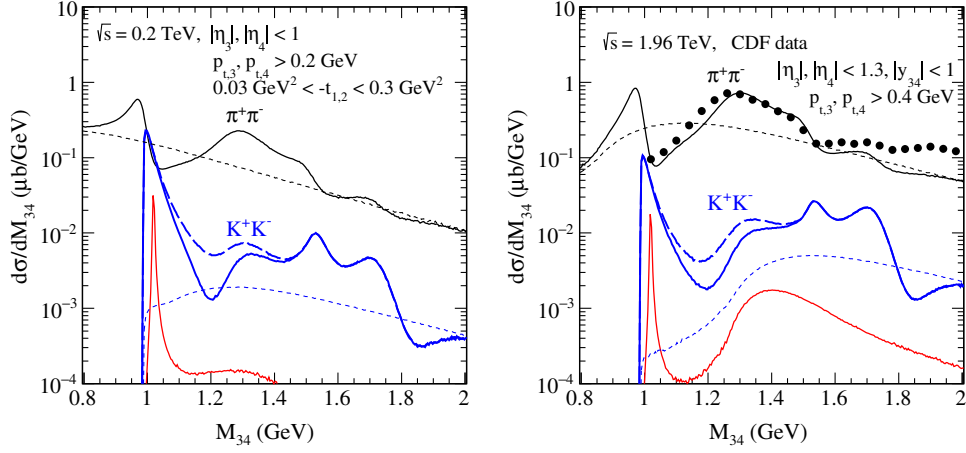


FIG. 9. The invariant mass distributions for centrally produced $\pi^+\pi^-$ (the black top lines) and K^+K^- (the blue bottom lines) pairs with the relevant experimental kinematical cuts specified in the legend. Results including both the nonresonant continuum and the resonances are presented. The short-dashed lines represent the purely diffractive continuum term. The solid and long-dashed blue lines correspond to the results for $\phi_{f_0(980)} = 0$ and $\pi/2$ in (5.1), respectively. The lower red line represents the $\phi(1020)$ meson plus continuum photoproduction contribution. The CDF experimental data from [20] in the right panel for the $p\bar{p} \rightarrow p\bar{p}\pi^+\pi^-$ reaction are shown for comparison. Absorption effects were taken into account effectively by the gap survival factors.

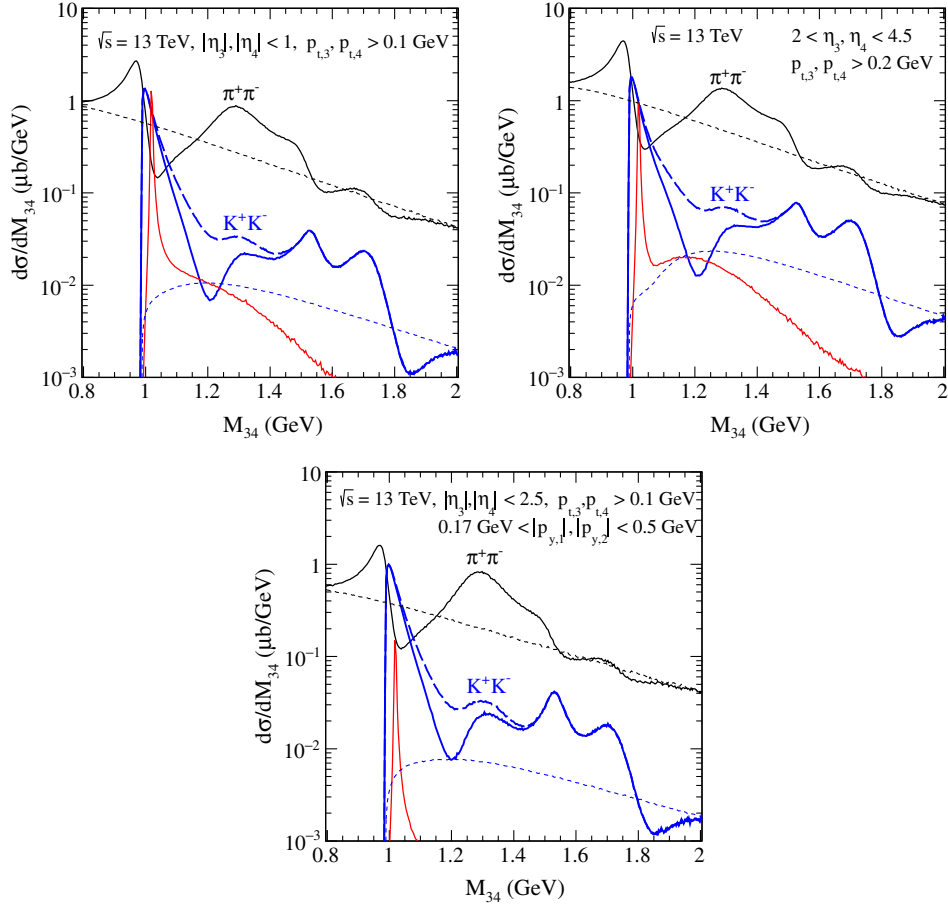


FIG. 10. The same as in Fig. 9 but for $\sqrt{s} = 13$ TeV and different experimental cuts specified in the legend. Absorption effects were taken into account effectively by the gap survival factors, $\langle S^2 \rangle = 0.1$ for the purely diffractive contribution and $\langle S^2 \rangle = 0.9$ for the photoproduction contribution.

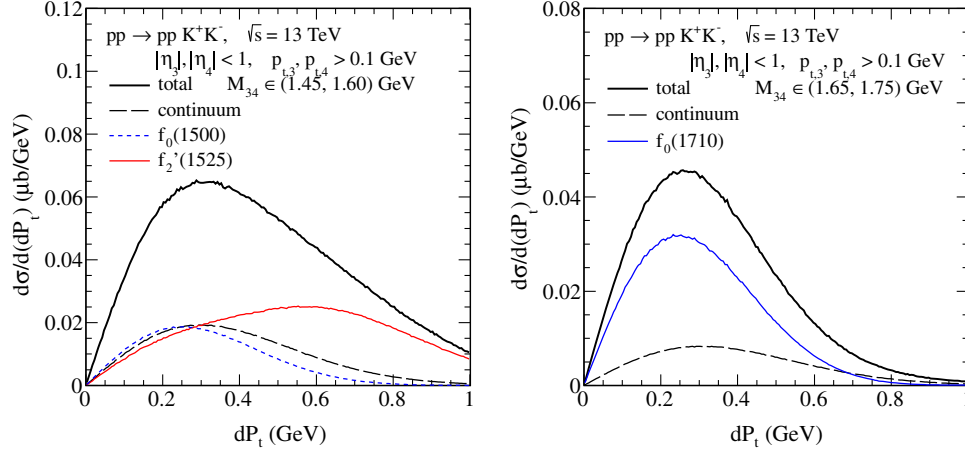


FIG. 11. The differential cross sections $d\sigma/d(dP_t)$ as a function of the dP_t “glueball filter” variable (3.61) for the $pp \rightarrow ppK^+K^-$ reaction. Calculations were done for $\sqrt{s} = 13$ TeV, $|\eta_K| < 1$, $p_{t,K} > 0.1$ GeV, and in two dikaon invariant mass regions, $M_{34} \in (1.45, 1.60)$ GeV and $M_{34} \in (1.65, 1.75)$ GeV, see the left panel and the right panel, respectively. Both, nonresonant continuum and resonances are included here. No absorption effects were taken into account here.

and the scalar $f_0(980)$, $f_0(1500)$, $f_0(1710)$, and tensor $f_2(1270)$, $f_2'(1525)$ resonances. For the $pp \rightarrow ppK^+K^-$ reaction we show predictions for $\phi_{f_0(980)} = 0$ and $\pi/2$ in (5.1), see the solid and long-dashed blue lines, respectively. The $f_0(980)$ resonance term in the $pp \rightarrow ppK^+K^-$ reaction is calculated with the upper limit for the coupling, $g_{f_0(980)K^+K^-} = 3.48$; see (3.45). The lower red lines show the photoproduction contributions. The diffractive and photoproduction contributions to K^+K^- production must be added coherently at the amplitude level and in principle could interfere. However, this requires the inclusion of absorption effects (at the amplitude level) that are different for both classes of processes, see e.g. [29]. In [28] we found that for the reaction $pp \rightarrow pp\pi^+\pi^-$ a similar interference effect is below 1%. The reader is asked to note different shapes of the $\pi^+\pi^-$ and K^+K^- invariant mass distributions for different experimental setups. In the left panel of Fig. 9 we show distributions for the STAR experiment. In the right panel we show results for the CDF experimental conditions together with data for the $p\bar{p} \rightarrow p\bar{p}\pi^+\pi^-$ reaction [20]. The limited CDF acceptance, in particular the $p_t > 0.4$ GeV condition on centrally produced K^+ and K^- mesons, causes a reduction of the cross sections in the region $M_{34} < 1.3$ GeV; see e.g. the clearly visible minimum for the photoproduction term there.

The calculations were done at Born level and the absorption corrections were taken into account by multiplying the cross section for the corresponding collision energy by a common factor $\langle S^2 \rangle$ obtained from [34,36]. For the purely diffractive contribution the gap survival factors $\langle S^2 \rangle = 0.2$ and 0.1 for $\sqrt{s} = 0.2$ TeV and 1.96 TeV, respectively, were taken. For the photoproduction contribution the Born calculation was multiplied by the factor

$\langle S^2 \rangle = 0.9$; see [29]. The absorption effects lead to a huge damping of the cross section for the purely diffractive contribution and a relatively small reduction of the cross section for the $\phi(1020)$ photoproduction contribution. Therefore we expect that one could observe the ϕ resonance term, especially when no restrictions on the leading protons are included. This situation is shown in Fig. 10, see the top left and right panels for the ALICE and LHCb experimental conditions, respectively. However, the final answer can only be given considering the experimental mass resolution of a given experiment. Here, for $\sqrt{s} = 13$ TeV, we take $\langle S^2 \rangle = 0.1$ for the purely diffractive contribution and $\langle S^2 \rangle = 0.9$ for the photoproduction contribution. In the bottom panel of Fig. 10 we show results with extra cuts on the leading protons of $0.17 \text{ GeV} < |p_{y,1}|, |p_{y,2}| < 0.5$ GeV as will be the momentum window for ALFA on both sides of the ATLAS detector [82]. Here the $\phi(1020)$ resonance is not so-well visible.

In Figs. 11 and 12 we present differential observables for the ALICE kinematics ($\sqrt{s} = 13$ TeV, $|\eta_K| < 1$, $p_{t,K} > 0.1$ GeV) and for two regions: $M_{34} \in (1.45, 1.60)$ GeV (the left panels) and $M_{34} \in (1.65, 1.75)$ GeV (the right panels). Figure 11 shows the distributions in the “glueball filter” variable dP_t ; see (3.61). We see that the maximum for the $q\bar{q}$ state $f_2'(1525)$ is around of $dP_t = 0.6$ GeV. On the other hand, for the scalar glueball candidates $f_0(1500)$ and $f_0(1710)$ the maximum is around $dP_t = 0.25$ GeV, that is, at a lower value than for the $f_2'(1525)$. This is in accord with the discussion in Sec. III C and in Ref. [9].

Angular distributions in the dimeson rest frame are often used to study the properties of dimeson resonances. Figure 12 shows the distribution of the cosine of $\theta_{K^+}^{r.f.}$,

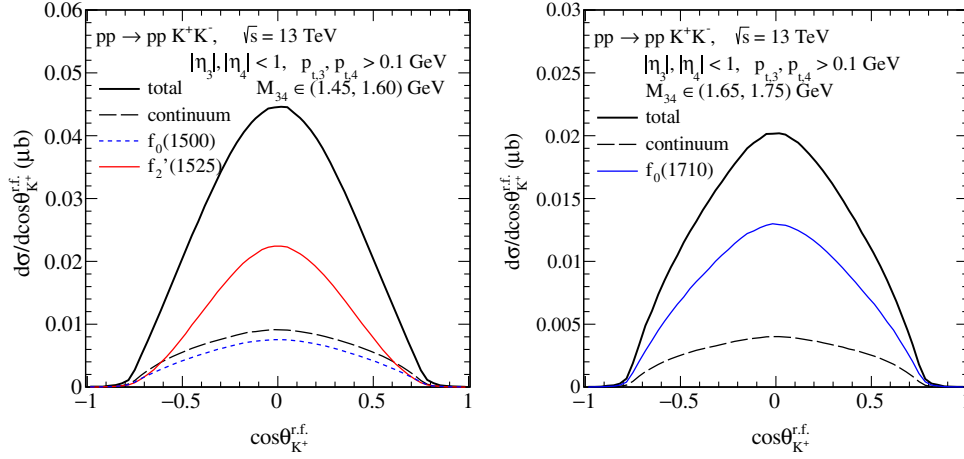


FIG. 12. The differential cross sections $d\sigma/d\cos\theta_{K^+}^{r.f.}$ as a function of the cosine of the polar angle $\theta_{K^+}^{r.f.}$ in the K^+K^- rest frame for the $pp \rightarrow ppK^+K^-$ reaction for two different windows of K^+K^- invariant mass. The predictions shown correspond to $\sqrt{s} = 13$ TeV and include cuts $|\eta_K| < 1$ and $p_{t,K} > 0.1$ GeV. The meaning of the lines is the same as in Fig. 11. No absorption effects were taken into account here.

the polar angle of the K^+ meson with respect to the beam axis, in the K^+K^- rest frame.⁵

It should be emphasized that our predictions were done with our choice of parameters collected in Table II. From the partial wave analysis, performed by the WA76/102 collaborations [10,11], more amount of the S -wave than of the D -wave in the mass region around 1.5 GeV was observed. This observation was confirmed by the E690 experiment [83] at the Fermilab Tevatron at $\sqrt{s} = 40$ GeV in the $pp \rightarrow p_{\text{slow}}K_S^0K_S^0p_{\text{fast}}$ reaction. This would change the behavior of invariant mass distribution around $M_{KK} = 1.5$ GeV. Note that the relative phase between K^+K^- -continuum and $f_0(1500)$ amplitudes is not so well determined and a constructive interference cannot be excluded. Here we do not show explicitly the corresponding result.

VI. CONCLUSIONS

We have discussed central exclusive production (CEP) of K^+K^- pairs in proton-proton collisions at high energies. We have taken into account purely diffractive and diffractive photoproduction mechanisms. For the purely diffractive mechanism we have included the continuum and the dominant scalar $f_0(980)$, $f_0(1500)$, $f_0(1710)$ and tensor $f_2(1270)$, $f_2'(1525)$ resonances decaying into K^+K^- pairs. The amplitudes have been calculated using Feynman rules within the tensor-Pomeron model [24]. The effective Lagrangians and the vertices for $\mathbb{P}\mathbb{P}$ fusion into the scalar and tensor mesons were discussed in [27,28], respectively. The model parameters of the Pomeron-Pomeron-meson

couplings have been roughly adjusted to recent CDF data [20] and then used for predictions for the STAR, ALICE, CMS and LHCb experiments. For the photoproduction of K^+K^- pairs we have discussed the dominant $\phi(1020)$ meson contribution and the nonresonant (Drell-Söding) contribution. Similar mechanisms were discussed in [29] for the $\pi^+\pi^-$ photoproduction. The coupling parameters of the tensor Pomeron to the ϕ meson have been fixed based on the HERA experimental data for the $\gamma p \rightarrow \phi p$ reaction [60,69].

In the present study we have focused mainly on the invariant mass distributions of centrally produced K^+K^- . In Fig. 9 we also presented, for comparison, the purely diffractive contribution previously developed in [28] for the central production of $\pi^+\pi^-$ pairs. The pattern of visible structures in the invariant mass distributions is related to the scalar and tensor isoscalar mesons and it depends on experimental kinematics. One can expect, with our default choice of parameters, that the scalar $f_0(980)$, $f_0(1500)$, $f_0(1710)$ and the tensor $f_2(1270)$, $f_2'(1525)$ mesons will be easily identified experimentally in CEP.

The ϕ -photoproduction and purely diffractive contributions have different dependences on the proton transverse momenta. Furthermore, the absorptive corrections for the K^+K^- photoproduction processes lead to a much smaller reduction of the cross section than for the diffractive ones. It can therefore be expected that the ϕ -photoproduction will be seen in experiments requiring only a very small deflection angle for at least one of the outgoing protons. However, we must keep in mind that other processes can contribute in experimental studies of exclusive ϕ production where only large rapidity gaps around the centrally produced ϕ meson are checked and the forward and backward going protons are not detected.

⁵It is also possible to consider a related observable, defined with respect to the Pomeron/Reggeon exchange three-vector; see e.g. [10,15].

Recently, experimental results for this kind of processes have been published by the CDF [20] and CMS [21] collaborations. We refer the reader to Ref. [31] in which ρ^0 production in pp collisions was studied with one proton undergoing diffractive excitation to an $n\pi^+$ or $p\pi^0$ system.

In addition, we have presented distributions in the so-called glueball filter variable, dP_t (3.61), which shows different behavior in the K^+K^- invariant mass windows around glueball candidates with masses ~ 1.5 GeV and ~ 1.7 GeV than in other regions. Also examples of angular distributions in the K^+K^- rest frame were shown. The dP_t distribution may help to interpret the relative rates between the $f_0(1500)$ and $f_2'(1525)$ resonances and to resolve the controversial discussion about the existence of the super-numerous resonances in the scalar sector [84].

Finally we note that central exclusive ϕ production in pp collisions offers the possibility to search for effects of the elusive Odderon, as was pointed out in [85]. The Odderon was introduced on theoretical grounds in [86,87]. For a review of Odderon physics see e.g. [88]. The experimental status of the Odderon is still unclear even if there seems to be some evidence for it from the recent TOTEM result [89]. For recent discussions of possible Odderon effects in pp elastic

scattering at LHC energies see [90–93]. Using the methods and results of the present paper it would be straightforward to include also ϕ production by Odderon-Pomeron fusion and to discuss Odderon effects, e.g. in K^+-K^- distributions, in a way analogous to the program presented in [30]. But this is beyond the scope of our present paper.

To summarize: we have given a consistent treatment of central exclusive K^+K^- continuum and resonance production in an effective field-theoretic approach. Our studies could help in understanding the production mechanisms of some light resonances and their properties in the $pp \rightarrow ppK^+K^-$ reaction. A rich structure has emerged which will give experimentalists interesting challenges to check and explore it.

ACKNOWLEDGMENTS

The authors are grateful to Leszek Adamczyk and Carlo Ewerz for discussions. This work was partially supported by the Polish National Science Centre Grants No. 2014/15/B/ST2/02528 and No. 2015/17/D/ST2/03530 and by the Center for Innovation and Transfer of Natural Sciences and Engineering Knowledge in Rzeszów, Republic of Poland/PL in Rzeszów.

-
- [1] T. Åkesson *et al.* (AFS Collaboration), A study of exclusive central hadron production at the ISR as a search for gluonium states, *Phys. Lett.* **133B**, 268 (1983).
 - [2] R. Waldi, K. R. Schubert, and K. Winter, Search for glueballs in a pomeron pomeron scattering experiment, *Z. Phys. C* **18**, 301 (1983).
 - [3] T. Åkesson *et al.* (AFS Collaboration), A search for glueballs and a study of double pomeron exchange at the CERN Intersecting Storage Rings, *Nucl. Phys.* **B264**, 154 (1986).
 - [4] A. Breakstone *et al.* (ABCDHW Collaboration), Production of the f^0 meson in the Double Pomeron Exchange reaction $pp \rightarrow pp\pi^+\pi^-$ at $\sqrt{s} = 62$ GeV, *Z. Phys. C* **31**, 185 (1986).
 - [5] A. Breakstone *et al.* (ABCDHW Collaboration), Inclusive Pomeron-Pomeron interactions at the CERN ISR, *Z. Phys. C* **42**, 387 (1989); Erratum **43**, 522 (1989).
 - [6] A. Breakstone *et al.* (ABCDHW Collaboration), The reaction Pomeron-Pomeron $\rightarrow \pi^+\pi^-$ and an unusual production mechanism for the $f_2(1270)$, *Z. Phys. C* **48**, 569 (1990).
 - [7] T. A. Armstrong *et al.* (WA76 Collaboration), Observation of centrally produced $\theta/f_2(1720)$ in the reaction $pp \rightarrow p_f(K\bar{K})p_s$ at 300 GeV/c, *Phys. Lett. B* **227**, 186 (1989).
 - [8] T. A. Armstrong *et al.* (WA76 Collaboration), Study of the centrally produced $\pi\pi$ and $K\bar{K}$ systems at 85 GeV/c and 300 GeV/c, *Z. Phys. C* **51**, 351 (1991).
 - [9] D. Barberis *et al.* (WA102 Collaboration), A kinematical selection of glueball candidates in central production, *Phys. Lett. B* **397**, 339 (1997).
 - [10] D. Barberis *et al.* (WA102 Collaboration), A partial wave analysis of the centrally produced K^+K^- and $K_S^0K_S^0$ systems in pp interactions at 450 GeV/c and new information on the spin of the $f_J(1710)$, *Phys. Lett. B* **453**, 305 (1999).
 - [11] B. R. French, A. Jacholkowski, J. B. Kinson, A. Kirk, O. Villalobos Baillie, M. F. Votruba, V. Lenti, and M. Stassinaki (WA76/102 Collaboration), A partial wave analysis of the centrally produced K^+K^- system in pp interactions at 300 GeV/c, *Phys. Lett. B* **460**, 213 (1999).
 - [12] D. Barberis *et al.* (WA102 Collaboration), A coupled channel analysis of the centrally produced K^+K^- and $\pi^+\pi^-$ final states in pp interactions at 450 GeV/c, *Phys. Lett. B* **462**, 462 (1999).
 - [13] D. Barberis *et al.* (WA102 Collaboration), Experimental evidence for a vector-like behavior of Pomeron exchange, *Phys. Lett. B* **467**, 165 (1999).
 - [14] D. Barberis *et al.* (WA102 Collaboration), A study of the $\eta\eta$ channel produced in central pp interactions at 450 GeV/c, *Phys. Lett. B* **479**, 59 (2000).
 - [15] A. Austregesilo (COMPASS Collaboration), A partial-wave analysis of centrally produced two-pseudoscalar final states in pp reactions at COMPASS, *Proc. Sci.*, (Bormio2013) (2013) 014, arXiv:1306.6814.

- [16] A. Austregesilo (COMPASS Collaboration), Light scalar mesons in central production at COMPASS, *AIP Conf. Proc.* **1735**, 030012 (2016).
- [17] A. Kirk, Resonance production in central pp collisions at the CERN Omega Spectrometer, *Phys. Lett. B* **489**, 29 (2000).
- [18] A. Kirk, A review of central production experiments at the CERN Omega spectrometer, *Int. J. Mod. Phys. A* **29**, 1446001 (2014).
- [19] M. G. Albrow, T. D. Coughlin, and J. R. Forshaw, Central exclusive particle production at high energy hadron colliders, *Prog. Part. Nucl. Phys.* **65**, 149 (2010).
- [20] T. A. Aaltonen *et al.* (CDF Collaboration), Measurement of central exclusive $\pi^+\pi^-$ production in $p\bar{p}$ collisions at $\sqrt{s} = 0.9$ and 1.96 TeV at CDF, *Phys. Rev. D* **91**, 091101 (2015).
- [21] V. Khachatryan *et al.* (CMS Collaboration), Exclusive and semi-exclusive $\pi^+\pi^-$ production in proton-proton collisions at $\sqrt{s} = 7$ TeV, Report Nos. CMS-FSQ-12-004, CERN-EP-2016-261.
- [22] L. Adamczyk, W. Guryn, and J. Turnau, Central exclusive production at RHIC, *Int. J. Mod. Phys. A* **29**, 1446010 (2014).
- [23] R. Sikora (STAR Collaboration), Central exclusive production in the STAR Experiment at RHIC, *AIP Conf. Proc.* **1819**, 040012 (2017).
- [24] C. Ewerz, M. Maniatis, and O. Nachtmann, A model for soft high-energy scattering: Tensor Pomeron and vector Odderon, *Ann. Phys. (Amsterdam)* **342**, 31 (2014).
- [25] C. Ewerz, P. Lebiedowicz, O. Nachtmann, and A. Szczurek, Helicity in proton-proton elastic scattering and the spin structure of the Pomeron, *Phys. Lett. B* **763**, 382 (2016).
- [26] L. Adamczyk *et al.* (STAR Collaboration), Single spin asymmetry A_N in polarized proton-proton elastic scattering at $\sqrt{s} = 200$ GeV, *Phys. Lett. B* **719**, 62 (2013).
- [27] P. Lebiedowicz, O. Nachtmann, and A. Szczurek, Exclusive central diffractive production of scalar and pseudoscalar mesons; tensorial vs. vectorial pomeron, *Ann. Phys. (Amsterdam)* **344**, 301 (2014).
- [28] P. Lebiedowicz, O. Nachtmann, and A. Szczurek, Central exclusive diffractive production of the $\pi^+\pi^-$ continuum, scalar, and tensor resonances in pp and $p\bar{p}$ scattering within the tensor Pomeron approach, *Phys. Rev. D* **93**, 054015 (2016).
- [29] P. Lebiedowicz, O. Nachtmann, and A. Szczurek, ρ^0 and Drell-Söding contributions to central exclusive production of $\pi^+\pi^-$ pairs in proton-proton collisions at high energies, *Phys. Rev. D* **91**, 074023 (2015).
- [30] A. Bolz, C. Ewerz, M. Maniatis, O. Nachtmann, M. Sauter, and A. Schöning, Photoproduction of $\pi^+\pi^-$ pairs in a model with tensor-pomeron and vector-odderon exchange, *J. High Energy Phys.* **01** (2015) 151.
- [31] P. Lebiedowicz, O. Nachtmann, and A. Szczurek, Central production of ρ^0 in pp collisions with single proton diffractive dissociation at the LHC, *Phys. Rev. D* **95**, 034036 (2017).
- [32] P. Lebiedowicz, O. Nachtmann, and A. Szczurek, Exclusive diffractive production of $\pi^+\pi^-\pi^+\pi^-$ via the intermediate $\sigma\sigma$ and $\rho\rho$ states in proton-proton collisions within tensor Pomeron approach, *Phys. Rev. D* **94**, 034017 (2016).
- [33] P. Lebiedowicz, O. Nachtmann, and A. Szczurek, Central exclusive diffractive production of $p\bar{p}$ pairs in proton-proton collisions at high energies, *Phys. Rev. D* **97**, 094027 (2018).
- [34] P. Lebiedowicz and A. Szczurek, $pp \rightarrow ppK^+K^-$ reaction at high energies, *Phys. Rev. D* **85**, 014026 (2012).
- [35] L. A. Harland-Lang, V. A. Khoze, and M. G. Ryskin, Modelling exclusive meson pair production at hadron colliders, *Eur. Phys. J. C* **74**, 2848 (2014).
- [36] P. Lebiedowicz and A. Szczurek, Revised model of absorption corrections for the $pp \rightarrow pp\pi^+\pi^-$ process, *Phys. Rev. D* **92**, 054001 (2015).
- [37] P. Lebiedowicz and A. Szczurek, Exclusive $pp \rightarrow pp\pi^+\pi^-$ reaction: From the threshold to LHC, *Phys. Rev. D* **81**, 036003 (2010).
- [38] A. Szczurek and P. Lebiedowicz, Exclusive scalar $f_0(1500)$ meson production for energy ranges available at the GSI Facility for Antiproton and Ion Research (GSI-FAIR) and at the Japan Proton Accelerator Research Complex (J-PARC), *Nucl. Phys.* **A826**, 101 (2009).
- [39] P. Lebiedowicz, R. Pasechnik, and A. Szczurek, Measurement of exclusive production of scalar χ_{c0} meson in proton-(anti)proton collisions via $\chi_{c0} \rightarrow \pi^+\pi^-$ decay, *Phys. Lett. B* **701**, 434 (2011).
- [40] R. Fiore, L. Jenkovszky, and R. Schicker, Exclusive diffractive resonance production in proton-proton collisions at high energies, [arXiv:1711.08353](https://arxiv.org/abs/1711.08353).
- [41] A. Cisek, W. Schäfer, and A. Szczurek, Exclusive photoproduction of ϕ meson in $\gamma p \rightarrow \phi p$ and $pp \rightarrow p\phi p$ reactions, *Phys. Lett. B* **690**, 168 (2010).
- [42] G. Sampaio dos Santos and M. V. T. Machado, Light vector meson photoproduction in hadron-hadron and nucleus-nucleus collisions at energies available at the CERN Large Hadron Collider, *Phys. Rev. C* **91**, 025203 (2015).
- [43] V. P. Goncalves, M. V. T. Machado, B. Moreira, F. S. Navarra, and G. Sampaio dos Santos, Color dipole predictions for the exclusive vector meson photoproduction in pp , pPb , and $PbPb$ collisions at run 2 LHC energies, *Phys. Rev. D* **96**, 094027 (2017), [arXiv:1710.10070](https://arxiv.org/abs/1710.10070).
- [44] C. Patrignani *et al.* (Particle Data Group), Review of particle physics, *Chin. Phys. C* **40**, 100001 (2016).
- [45] A. Donnachie and P. V. Landshoff, Total cross sections, *Phys. Lett. B* **296**, 227 (1992).
- [46] A. Donnachie, H. G. Dosch, P. V. Landshoff, and O. Nachtmann, Pomeron physics and QCD, *Cambridge Monogr. Part. Phys., Nucl. Phys., Cosmol.* **19**, 1 (2002).
- [47] J. Z. Bai *et al.* (BES Collaboration), Structure Analysis of the $f_J(1710)$ in the Radiative Decay $J/\psi \rightarrow \gamma K^+ K^-$, *Phys. Rev. Lett.* **77**, 3959 (1996).
- [48] J. Z. Bai *et al.* (BES Collaboration), Partial wave analyses of $J/\psi \rightarrow \gamma K^+ K^-$ and $\gamma K_S^0 K_S^0$, *Phys. Rev. D* **68**, 052003 (2003).
- [49] B. Aubert *et al.* (BABAR Collaboration), Dalitz plot analysis of the decay $B^\pm \rightarrow K^\pm K^\pm K^\mp$, *Phys. Rev. D* **74**, 032003 (2006).
- [50] D. V. Bugg, B. S. Zou, and A. V. Sarantsev, New results on $\pi\pi$ phase shifts between 600 and 1900 MeV, *Nucl. Phys.* **B471**, 59 (1996).
- [51] M. Albaladejo and J. A. Oller, Identification of a Scalar Glueball, *Phys. Rev. Lett.* **101**, 252002 (2008).

- [52] M. Ablikim *et al.* (BES Collaboration), Partial wave analyses of $J/\psi \rightarrow \gamma\pi^+\pi^-$ and $\gamma\pi^0\pi^0$, *Phys. Lett. B* **642**, 441 (2006).
- [53] S. Dobbs, A. Tomaradze, T. Xiao, and K. K. Seth, Comprehensive study of the radiative decays of J/ψ and $\psi(2S)$ to pseudoscalar meson pairs, and search for glueballs, *Phys. Rev. D* **91**, 052006 (2015).
- [54] F. E. Close and A. Kirk, Glueball— $q\bar{q}$ filter in central hadron production, *Phys. Lett. B* **397**, 333 (1997).
- [55] M. Poppe, Exclusive hadron production in two photon reactions, *Int. J. Mod. Phys. A* **01**, 545 (1986).
- [56] A. Szczurek and J. Speth, Perturbative QCD versus pion exchange and hadronic FSI effects in the $\gamma\gamma \rightarrow \pi^+\pi^-$ reaction, *Nucl. Phys. A* **728**, 182 (2003).
- [57] M. Kłusek-Gawenda and A. Szczurek, $\pi^+\pi^-$ and $\pi^0\pi^0$ pair production in photon-photon scattering in ultraperipheral ultrarelativistic heavy ion collisions, *Phys. Rev. C* **87**, 054908 (2013).
- [58] M. Kłusek-Gawenda, P. Lebiedowicz, O. Nachtmann, and A. Szczurek, From the $\gamma\gamma \rightarrow p\bar{p}$ reaction to the production of $p\bar{p}$ pairs in ultraperipheral ultrarelativistic heavy-ion collisions at the LHC, *Phys. Rev. D* **96**, 094029 (2017).
- [59] A. Cisek, P. Lebiedowicz, W. Schäfer, and A. Szczurek, Exclusive production of ω meson in proton-proton collisions at high energies, *Phys. Rev. D* **83**, 114004 (2011).
- [60] M. Derrick *et al.* (ZEUS Collaboration), Measurement of elastic ϕ photoproduction at HERA, *Phys. Lett. B* **377**, 259 (1996).
- [61] J. Ballam *et al.*, Vector-meson production by polarized photons at 2.8, 4.7, and 9.3 GeV, *Phys. Rev. D* **7**, 3150 (1973).
- [62] D. C. Fries, P. Heine, H. Hirschmann, A. Markou, E. Seitz, H.-J. Behrend, W. P. Hesse, W. A. McNeely, and T. Miyachi, S-P wave interference in K^+K^- photoproduction near K^+K^- threshold, *Nucl. Phys. B* **143**, 408 (1978).
- [63] R. M. Eglhoff *et al.*, Measurements of Elastic ρ^- and ϕ -Meson Photoproduction Cross Sections on Protons from 30 to 180 GeV, *Phys. Rev. Lett.* **43**, 657 (1979).
- [64] D. Aston *et al.* (Bonn-CERN-Ecole Poly-Glasgow-Lancaster-Manchester-Orsay-Paris-Rutherford-Sheffield Collaboration), Photoproduction of K^+K^- pairs on hydrogen at photon energies of 20 to 36 GeV, *Nucl. Phys. B* **172**, 1 (1980).
- [65] D. P. Barber *et al.*, A study of elastic photoproduction of low mass K^+K^- pairs from hydrogen in the energy range 2.8–4.8 GeV, *Z. Phys. C* **12**, 1 (1982).
- [66] M. Atkinson *et al.* (Omega Photon Collaboration), Photoproduction of ϕ mesons by linearly polarized photons of energy 20–40 GeV and further evidence for a photoproduced high-mass KK enhancement, *Z. Phys. C* **27**, 233 (1985).
- [67] J. Busenitz *et al.*, High-energy photoproduction of $\pi^+\pi^-\pi^0$, K^+K^- , and $p\bar{p}$ states, *Phys. Rev. D* **40**, 1 (1989).
- [68] J. M. Laget, Photoproduction of vector mesons at large momentum transfer, *Phys. Lett. B* **489**, 313 (2000).
- [69] J. Breitweg *et al.* (ZEUS Collaboration), Measurement of diffractive photoproduction of vector mesons at large momentum transfer at HERA, *Eur. Phys. J. C* **14**, 213 (2000).
- [70] E. M. Levin and L. L. Frankfurt, The quark hypothesis and relations between cross sections at high energies, *JETP Lett.* **2**, 65 (1965).
- [71] H. J. Lipkin and F. Scheck, Quark Model for Forward Scattering Amplitudes, *Phys. Rev. Lett.* **16**, 71 (1966).
- [72] H. J. Lipkin, Quark Models and High-Energy Scattering, *Phys. Rev. Lett.* **16**, 1015 (1966).
- [73] J. J. J. Kokkedee and L. Van Hove, Quark model and high-energy scattering, *Nuovo Cim.* **42**, 711 (1966).
- [74] H. J. Lipkin, New systematics in hadron total cross sections, *Phys. Rev. D* **11**, 1827 (1975).
- [75] R. M. Eglhoff, Measurements of elastic Rho, Omega and Phi meson photoproduction cross sections on protons from 30 to 180 GeV. PhD thesis, Toronto U., 1979. http://lss.fnal.gov/cgi-bin/find_paper.pl?thesis-1979-16.
- [76] A. I. Titov and T. S. H. Lee, Spin effects and baryon resonance dynamics in ϕ meson photoproduction at few GeV, *Phys. Rev. C* **67**, 065205 (2003).
- [77] B.-G. Yu, H. Kim, and K.-J. Kong, Role of σ exchange in the $\gamma p \rightarrow \phi p$ process and scaling with the f_1 axial vector meson from a Reggeized model, *Phys. Rev. D* **95**, 014020 (2017).
- [78] B. Dey, C. A. Meyer, M. Bellis, and M. Williams (CLAS Collaboration), Data analysis techniques, differential cross sections, and spin density matrix elements for the reaction $\gamma p \rightarrow \phi p$, *Phys. Rev. C* **89**, 055208 (2014); *Phys. Rev. C* Erratum **90**, 019901 (2014).
- [79] K. Mizutani *et al.* (LEPS Collaboration), ϕ photoproduction on the proton at $E_\gamma = 1.5$ –2.9 GeV, *Phys. Rev. C* **96**, 062201 (2017).
- [80] D. Melikhov, O. Nachtmann, V. Nikonov, and T. Paulus, Masses and couplings of vector mesons from the pion electromagnetic, weak, and $\pi\gamma$ transition form factors, *Eur. Phys. J. C* **34**, 345 (2004).
- [81] R. A. Kycia, J. Chwastowski, R. Staszewski, and J. Turnau, GenEx: A simple generator structure for exclusive processes in high energy collisions, [arXiv:1411.6035](https://arxiv.org/abs/1411.6035).
- [82] L. Adamczyk (private communication).
- [83] M. A. Reyes *et al.* (E690 Collaboration), Partial Wave Analysis of the Centrally Produced $K_S K_S$ System at 800 GeV/c, *Phys. Rev. Lett.* **81**, 4079 (1998).
- [84] W. Ochs, The status of glueballs, *J. Phys. G* **40**, 043001 (2013).
- [85] A. Schäfer, L. Mankiewicz, and O. Nachtmann, Double-diffractive J/ψ and ϕ production as a probe for the odderon, *Phys. Lett. B* **272**, 419 (1991).
- [86] Ł. Łukaszuk and B. Nicolescu, A possible interpretation of pp rising total cross-sections, *Lett. Nuovo Cimento Soc. Ital. Fis.* **8**, 405 (1973).
- [87] D. Joynson, E. Leader, B. Nicolescu, and C. Lopez, Non-regge and hyper-regge effects in pion-nucleon charge exchange scattering at high energies, *Nuovo Cim. Soc. Ital. Fis.* **30A**, 345 (1975).
- [88] C. Ewerz, The Odderon in quantum chromodynamics, [arXiv:hep-ph/0306137](https://arxiv.org/abs/hep-ph/0306137).
- [89] G. Antchev *et al.* (TOTEM Collaboration), First determination of the ρ parameter at $\sqrt{s} = 13$ TeV—probing the existence of a colourless three-gluon bound state, Report No. CERN-EP-2017-335, 2017.

-
- [90] E. Martynov and B. Nicolescu, Did TOTEM experiment discover the Odderon?, *Phys. Lett. B* **778**, 414 (2018).
- [91] V. A. Khoze, A. D. Martin, and M. G. Ryskin, Elastic proton-proton scattering at 13 TeV, *Phys. Rev. D* **97**, 034019 (2018).
- [92] V. A. Khoze, A. D. Martin, and M. G. Ryskin, Black disk, maximal Odderon and unitarity, *Phys. Lett. B* **780**, 352 (2018).
- [93] M. Broilo, E. G. S. Luna, and M. J. Menon, Soft pomerons and the forward LHC data, *Phys. Lett. B* **781**, 616 (2018).